ATMOSPHERIC, OCEANIC
AND PLANETARY PHYSICS
UNIVERSITY OF OXFORD

DPhil Second Year Report

# Studies of Venus using a General Circulation Model

João Manuel Mendonça

Supervisor
Prof. Peter L. Read

Co-Supervisor
Dr. Stephen R. Lewis
(The Open University)

August 2010

E-mail: Mendonca@atm.ox.ac.uk
Number of Words: $\sim$ 13000

## Studies of Venus using a General Circulation Model

**Abstract:** The main objective of my DPhil is to study and understand the atmospheric circulation of slowly rotating "planets" such as Venus and Titan, that despite their differences, exhibit super rotating atmospheres and other similar features in their atmospheres.

In this report I present our latest work where the Venus Simplified General Circulation Model (SGCM) was used to explore and understand the Venus' atmospheric circulation and to explore the accuracy of a thermal zonal wind retrieval method for the Venus' mesosphere. We also present the most recent code's structure and results on the Titan SGCM, which will be an important tool to understand the super rotating atmosphere in slowly rotating planets. Finally, we present the proposed new radiative transfer formulation to be included in the Venus General Circulation Model (GCM).

This report is a description of the work done, and is structured as follows: I first write an introduction, followed by the results of the research we have done for each Astronomical object (Venus and Titan), and finally present a summary of my future plan of work.

# Contents

# List of Figures

# List of Tables

CHAPTER 1

# Introduction

## Contents



## 1.1 Modeling Venus' Atmospheric Circulation

The Venus climate community has been benefiting from the advances in modelling the Earth's atmosphere and also from the experience of adapting those models to Mars's atmosphere. The dynamical and physical parameterisations involved in the development of a GCM for Telluric planets like Earth, Mars and Venus are very similar. The main differences are in the physics packages where we need to define the characteristics of the planets (solid body and atmospheric parameters) and/or use simplified parameterisations due to lack of observations or to reduce the computational time of these complex models.

Simplified General Circulation Models (SGCMs) applied to the planet Venus have become important tools for understanding its atmospheric dynamics, and are being developed now by several groups across the world. These models do not try to use full physical representations of all process, but include simplified representations of heating, cooling and friction processes to simulate the circulation of Venus's atmosphere, that is well known to exhibit strong super-rotation and a variety of enigmatic features which remain poorly understood. Previous work in Oxford (Lee [2006] and Lee et al. [2007]) has resulted in the development of a SGCM, which is already capable of qualitatively producing plausible realistic Venus-like global circulations, with a significant super-rotation (within a factor of 2).

Venus models are at the stage of evolving from SGCMs towards more complete and physically-based ones. The process is complex and challenging due to difficulties in reproducing the global atmosphere of Venus in a realistic numerical approach. To date, the French (LMD, Paris, France) GCM (Lebonnois et al. 2010b) is the only attempt to include a full radiative transfer model that computes temperature structure self-consistently. This is particularly challenging because of the extreme opacity of the atmosphere in the IR, which makes the fast computation of accurate results difficult. The method used in the

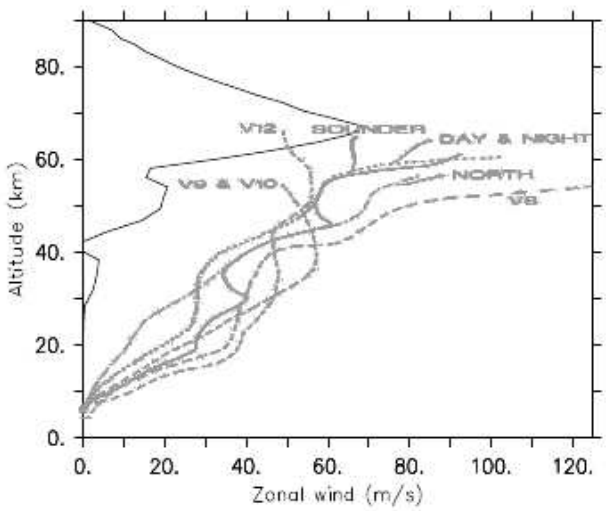


Figure 1.1: The black line represents the vertical profile of the zonally averaged zonal wind at the equator from the LMD Venus GCM, Lebonnois et al. [2010b]. The others lines were obtained from the Venera and Pioneer Venus missions, Schubert [1983].

LMD group is based on the parameterisation developed by Eymet et al. [2009], that uses a Net Exchange Rates formulation for the thermal radiation and tables of fluxes for the solar radiation (Crisp [1986]). This is the most successful recent model, and seems capable of showing a super-rotation above the clouds similar to observations. Below the clouds, the results have not been so successful since when starting from an initial condition at rest the observed variation with height of the super-rotation is not obtained (Figure 1.1). Below in this report, in the new radiative scheme section (using similar parameterisation to the one used in the GCM of the LMD group), it is possible to observe that the mid atmosphere (55 to 100 km) is heated from the hot lower atmosphere (0 to 55 km), creating a zone of convection. The cooling to space appears to be stronger at the upper atmosphere, inducing thermal instabilities. There are several points to be investigated using complete models like the LMD model, such as (a) the role of the thermal tides which seem to be important to maintain a strong equatorial super-rotation in the LMD GCM, (b) the influence of variations of the specific heat with temperature, (c) the role of the topography and (d) the potential role of sub-grid scale gravity waves.

This report describes the radiative transfer formulation that has been developed for the Oxford Venus GCM and also some studies concerning the Venus' atmospheric circulation using the SGCM. The new implementation will turn the Oxford model into one of the most advanced models to date to study the Venus atmosphere, computing the cooling/heating rates self-consistently for the solar and thermal radiation.

## 1.2 Dynamical Problems of the Venus's Atmosphere

### 1.2.1 Overview

The circulation of the atmosphere on Venus is governed by two regimes for different structures in the atmosphere: the retrograde zonal super-rotation in the troposphere and mesosphere [Read, 1986], and the solar-antisolar circulation across the terminator in the thermosphere [Bougher et al., 1997]. Several observations made by descent probes, Vega balloons or using cloud tracking in the UV, showed that in the troposphere (0 to around 70km), the winds reach a maximum of 100ms$^{-1}$ at the cloud tops and decrease to roughly zero at the surface (Schubert [1983]). On average, the main cloud deck rotates around the planet in a period of 4-5 days, being around 50-60 times faster than the rotation of the solid planet body, with a maximum of 2m$s^{-1}$ at the equator relative to the background stars.

The dynamics of the atmosphere on Venus is driven by a differential spatial insolation, and the presence of mid or high latitude super-rotation is well explained as a consequence of poleward angular momentum transport by a thermally direct Hadley circulation. More difficult to explain, is the presence of the observed equatorial super-rotation in its atmosphere. Such a phenomenon requires the presence of nonaxisymmetric eddy motions, because the flow in this zone rotates with much higher angular velocity than in an axisymmetric circulation, unless super-rotation was its initial condition. There are several mechanisms that can explain the formation of such eddies: a barotropic instability of a high-latitude jet produced by the Hadley cell (Gierasch [1975] and Rossow and Williams [1979]); transient or topographically forced planetary or small-scale gravity waves [Leovy, 1973]; a Solar semidiurnal thermal tide [Fels and Lindzen, 1974].

The polar vortex structure has been observed over three decades, centered over the pole and thought to be similar in each hemisphere, with characteristics very similar to those of a Rankine vortex. Is the Venus vortex a permanent feature of the Venus atmosphere like the super-rotation? And how are they both linked? These are two questions that remain poorly understood. The zonal winds that characterized this vortex at the cloud level (65-70km) increase from the equator to 45° latitude and then weaken up to the pole to values similar to the rotation of a rigid body.

The observations in the IR made by Venus Express showed a bright south pole surrounded by a cold "collar" [Piccioni et al., 2007], that is very similar to what was observed in previous missions to the north pole [Taylor et al., 1979]. These huge cyclonic structures change their central morphology continually, showing a single, double or tri-vortex structure that rotates around the pole. The dynamics of the polar vortices on Venus seem to be related to the possibility of barotropic instabilities in the polar flow [Limaye et al., 2009]. Analysing in altitude, there are two phases that characterise the polar vortex: at about 50 km, a cold "collar" circulating around a higher temperature polar cap, and at about 90 km, a warm pole, where the temperature of the pole is higher than the equator.

The nature and mechanisms underlying the polar temperature structures and the polar vortices are still not clear. It has been proposed that the polar temperature structures are a result of the compressional adiabatic warming from the descending branch of the meridional cell circulation, coupled with variations in the solar heating, due to changes in the

haze densities at 80 km.

The global waves activity in Venus' atmosphere is likely to play an important role in the transport of momentum and energy in the atmosphere. The planetary-scale cloud patterns observed in the UV measurements, with a shape of a large horizontal "Y", can be explained by the presence of atmospheric waves travelling slowly with respect to the cloud-top winds. The combination of mid latitude waves travelling somewhat slower than the winds and interfering with slightly faster equatorial waves, coupled with some non-linear effects, can explain the pattern observed. The real nature of the waves in the atmosphere of Venus is difficult to explain due to the lack of observational data. Del Genio and Rossow [1990] studied the images in the UV to study the characteristics of the waves in the atmosphere of Venus, and correlated the contrasts of an unknown absorber ("Y" and reversed "C" shape), the winds and the temperature fields. The waves observed at 65-70 km of altitude were of two types: equatorially trapped waves moving in the same direction as the wind but faster, extending from its equator to roughly 20° latitude and with a period of 4 days, identified as a equatorial Kelvin wave; mid-latitude waves moving in the same direction of the winds but slower, with two different periods of 4 and 5.2 days, which were intrepreted as Mixed-Rossby-Gravity waves [Del Genio and Rossow, 1990].

### 1.2.2 Questions

The main challenge in my DPhil project is to simulate and gain a better understanding of the atmospheric super-rotation of the Venus' atmosphere. A main question rises while studying this phenomenon as was pointed out in the previous subsection:

- What is the real mechanism that drives a slowly rotating planet like Venus to have a super-rotating atmosphere?

There are a number of key scientific question that need to be answered to understand the real nature of this general type of planetary circulation, since it is also observed in Titan. Despite differences in the physical body, different rates of vertical and horizontal profiles of heating and cooling (Venus: important diurnal variations; Titan: important seasonal variations) and the amount of total atmospheric mass, both rotate slowly and produce a super-rotating atmosphere. A SGCM for this secondary planet (section 2) has been developed since it can help us to understand the science beyond this fast rotation and help us to have more tools to answer important questions such as:

- Is the super-rotation an inevitable state of slow rotating planets?
- What are the atmospheric parameters for which the atmosphere is sensitive to in its transition to super-rotation?
- Are phenomena, such as the polar vortex or the large-scale wave patterns observed in the atmosphere of Venus, common in super-rotating atmospheres?
- Which types of waves are most important for sustaining super-rotation? - Planetary waves, Gravity waves or Thermal tides?

- What is the role of topography and surface interactions?
- What is the role of seasonal variations, which are much larger on Titan than on Venus?
- What is the dynamical role of clouds either as passive or active factors? Also, what determines the distribution and properties of clouds across the planet? The model used in this work [Lee et al., 2010b], obtains a cloud distribution similar to observations.

These are some of the questions that we would like to study in this project, developing and exploring numerical models capable of reproducing the Venus atmospheric dynamics. A better understanding of the Venus Meteorology will have consequently an important role in interpreting the observational data from previous and future observational missions.

## 1.3 Report Summary

In the next Chapter, I will give an overview of the SGCM for Venus and Titan, and describe the simplified parameterisation for heating, cooling and friction used.

Chapter 3 describes the work done using the SGCM for Venus to study the nature of the flow mainly in the polar regions. It also investigates the sensitivity of the retrieved zonal flow to the lower boundary conditions in the upward integration of the thermal wind equation.

Chapter 4 describes the new solar and thermal radiation code that has been developed to be implemented in the Oxford Venus GCM.

A general conclusion of my first year and a brief summary about my future work are presented in Chapters 5 and 6.

CHAPTER 2

# Simple General Circulation Models

## Contents



## 2.1 Simple Venus GCM

The Venus SGCM used in this work was developed in Oxford [Lee, 2006], and is also known as OPUS-V (**O**xford **P**lanetary **U**nified **S**imulation model for **V**enus). This model was based in an advanced GCM, the Unified Model developed in the United Kingdom Meteorological Office [Cullen et al., 1992], and adapted for the study of the atmosphere of Venus [Lee et al., 2007].

### 2.1.1 Basis

The Venus GCM uses values of the physical and dynamical properties corresponding to Venus (Colin [1983] and Williams [2003b]), and simplified parameterisations for radiative forcing and boundary layer dissipation. It is configured on an Arakawa B grid [Arakawa and Lamb, 1981], and adapted to use a 5°x5° horizontal resolution covering the entire domain with 31 vertical levels, extended from the surface to an altitude of around 90 km, with a maximum of 3.5 km in the vertical grid spacing.

The radiation scheme used is not based on a radiative transfer model. It uses a linear temperature relaxation scheme towards a global-averaged reference temperature profile, obtained from Pioneer Venus probe data [Seiff et al., 1980], plus a perturbation function that gives the equator-to-pole differences for each altitude, chosen to give qualitatively the peak in absorption of solar insulation within the cloud deck (Tomasko et al. 1985; Lee 2006; Lee et al. 2007). The interaction of the atmosphere with the surface was modelled by a boundary layer scheme with a linearised friction parameterisation. In the three upper layers, a sponge layer is included, with Rayleigh friction damping the horizontal eddy component of winds to zero.

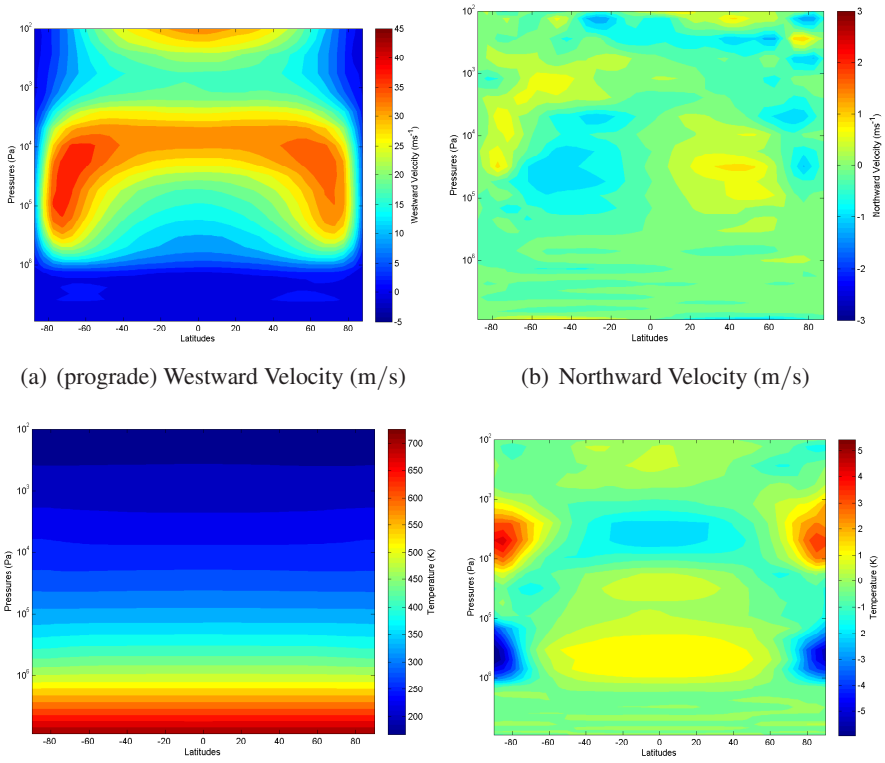


(a) (prograde) Westward Velocity (m/s)

(b) Northward Velocity (m/s)

(c) Temperature (K)

(d) Temperature (K)

Figure 2.1: Prognostic variable after 500 Earth days of zonal average from the Oxford Venus SGCM without the diurnal forcing, and after 41000 Earth days of integration from a rest atmosphere. **(a)** Westward wind speed (m/s). **(b)** Northward wind speed (m/s). **(c)** Temperature (K). **(d)** Temperature (K) after the latitude mean has been removed.

Using this simple GCM for Venus, it was possible to reproduce a super-rotating atmosphere without any non-physical forcing, diurnal or seasonal cycles. The result of the super-rotation is shown in Figure 2.1(a), where the horizontal equatorward transport of momentum at 40-80 km is responsible for maintaining the equatorial super-rotation (Lee [2006]).

The model reproduces equatorial Kelvin waves and Mixed-Rossby-Gravity (MRG) waves spontaneously, as shown in Figure 2.2. Regarding the MRG waves, it was verified that they have an important influence in maintaining the equatorial super-rotation.

In Figure 2.1(d), it is possible to observe in the polar region that the model reproduces qualitatively the “cold collar" in the middle atmosphere and a warm pole in the upper atmosphere.

The model implements a passive tracer parameterisation which includes: condensation, evaporation and sedimentation of a mono-modal sulphuric acid cloud. The condensation and evaporation are two instantaneous processes, determined by the saturation vapour pressure (SVP) profile for acid sulphuric vapour. The sedimentation rates are determined by the pressure dependent viscosity of carbon dioxide, where it is assumed that particles fall at

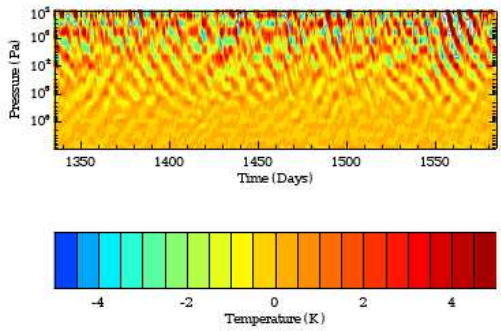


(a) Equatorial Kelvin waves

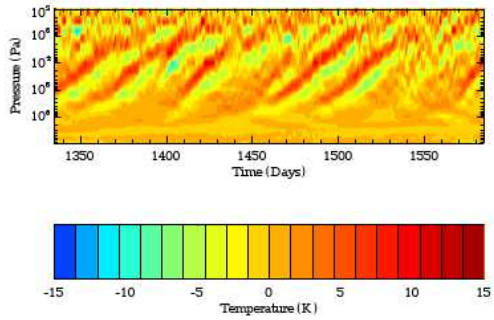


(b) Mixed-Rossby-Gravity waves

Figure 2.2: **(a)** Equatorial Kelvin waves with a period of 9.5±0.5 days and **(b)** Mixed-Rossby-Gravity waves with periods of 30±2 days are spontaneously produced in the model (Lee 2006). The results for the temperature anomaly were taken at a longitude point of 65°N, and at the equator. The time axis represents the time integration of the model in Earth days.

their terminal Stokes velocity (Lee et al. [2010a] and Lee [2006]). Using this passive tracer scheme, large structures in the atmosphere very similar to those observed were found: the "Y" shape and reversed "C" shape features. The model includes also an ideal diurnal cycle parameterisation. The simple formulation perturbs the thermal relaxation field in a form of a "hot spot" that varies with the Sun's position, creating diurnal and semi-diurnal tides in the atmosphere. The equatorward momentum transport due to these tides maintains the equatorial super-rotation in the model and produces a stronger global super-rotation.

A more complex boundary layer was tested in the model: a Monin-Obukhov boundary layer parameterisation, which was integrated with a realistic topography for Venus. Nevertheless the results did not show any significant influence in the global mean circulation.

### 2.1.2 Simple Parameterisation

#### 2.1.2.1 Temperature Forcing

Due to the difficulties in implementing a complex and fast radiative transfer model suitable for a Venus GCM, the Oxford model uses a linear temperature relaxation instead [Lee, 2006]. This parameterisation forces the temperature towards a radiative equilibrium atmosphere at each point ($\lambda$-longitude, $\phi$-latitude, p-pressure, t-time) of the SGCM grid using,

$$\delta T_{rad}(\lambda, \phi, p, t) = -\frac{T(\lambda, \phi, p, t) - T_0(\phi, p)}{\tau}\delta t \tag{2.1}$$

where $T_0(\phi,p)$ is the forcing temperature structure which gives the differences in temperature equator-to-pole, and $\tau$ is the time constant in this formulation.

The form of the relaxation temperature is,

$$T_0(\phi, p) = T_{ref}(p) + T_1(p)(cos(\phi) - C). \tag{2.2}$$

In this equation we find $T_{ref}(p)$ which is the reference temperature profile obtained from Seiff et al. [1980] and Seiff [1983], $T_1(p)$ is a perturbation term that shapes the equator-to-pole difference, and finally the constant C which is the result of forcing the integral of cos($\phi$) - C to be zero over the domain (C = $\frac{\pi}{4}$). The values of $T_1(p)$ are chosen to give qualitatively the influence of the peak in absorption of solar insulation within the cloud deck [**?**]. The values for the time constant used are smaller than the values observed for the atmosphere of Venus to save computational time, and it is expected to have the same effect as large values. The true values for the relaxation time-scale are difficult to obtain due to the large value near the surface which could induce the observation of false values. The values for $\tau$ are 25 Earth days, decreasing slightly in the uppermost levels.

#### 2.1.2.2 Boundary Layer Scheme

The surface boundary layer parameterisation used in the Venus GCM simulates the interaction between the surface and the atmosphere, and is based in a linear friction parameter-

isation which is fairly correct for Venus conditions [Lee, 2006]. This simple formulation was constructed using,

$$\frac{d\vec{u}}{dt} = -\frac{\vec{u}}{\tau_d}, \tag{2.3}$$

where $\tau_d$ is the relaxation time scale and $\vec{u}$ is the horizontal velocity vector at the lowest layer only (the velocity at the surface level is assumed to be equal to zero). The planet's surface is assumed to be flat, so the value for $\tau_d$ is the same at all the surface points, 32 Earth days, which using a relation between the relaxation period and the bulk transfer coefficients gives approximately the typical values for the Earth [Lee, 2006].

At the top three layers of the GCM, a sponge layer is included, with the same Rayleigh friction damping the eddy components of the velocity field, to avoid the reflection of any wave in the numerically imposed rigid lid. The time constants were chosen from values between 100 and 0.01 Earth days, decreasing with altitude in the GCM grid.

## 2.2 Simple Titan GCM

We have developed a simplified atmospheric model to study the climate of Titan based on the Venus SGCM. The absence of a radiative transfer formulation does not make this new model as one of the most complex GCM applied to Titan (see Hourdin et al. 1995). The aim of this work is to study qualitatively the dynamics of its atmosphere which shows some similarities to the dynamics of Venus, as well as the importance of the seasonal effects in the super-rotation. It is important to understand what are the responsible mechanisms for the super-rotation and if it is an inevitable condition of the slow body rotation.

The simplicity of the parameterisations will roughly be the same as the Venus SGCM, which can help to study their versatility to different conditions and perhaps improve them.

### 2.2.1 Basis

The OPUS-T (**O**xford **P**lanetary **U**nified **S**imulation model for **T**itan) was developed from an adaptation of the previous Venus model ([Lee et al., 2007]), where the physical and dynamical conditions were changed to better suit Titan.

### 2.2.2 Simple Parameterisations

#### 2.2.2.1 Basic Parameters

The present Titan SGCM uses the same boundary layer as the Venus SGCM and an adapted temperature forcing. The variable characteristic of its motion and physical characteristics properties are in the Table 2.1, and the resolution used is: 37x72 horizontal per 54 vertical levels covering 500 km (Table 2.2).The vertical resolution (sigma levels) is the same used in Rannou et al. [2005]. The ellipticity of Saturn's orbit around the Sun was neglected and it was assumed that it is in synchronous orbit around Saturn. Maintaining the same horizontal resolution and time step as the Venus model, we are still satisfying the CFL (Courant-Friedrichs-Lewy) condition, which filters any zonal winds which are too fast comparing with the wind speeds for that latitude position. As Titan's radius ($r_T$) is less than the Venus radius, the running of Titan's model becomes more unstable (potential temperature and surface pressure appear negative in several points of the GCM grid), keeping the same time step ($\Delta$t), horizontal resolution ($\Delta\phi$) and the strength of the diffusion (K). These values should obey the stability criterion (Cullen et al. [1992]),

$$\Delta t(\frac{4K}{{r_T}^2\Delta\phi^2})^j \leq 1, \tag{2.4}$$

where j is related with the order of diffusion, from the numerical eddy diffusion routine which filters the entire model domain (j=3, gives an order of diffusion equal to 6). This criterion limits the values of K that ensure a stable model, which are for all the altitudes less than the values used for Venus, since the other variables in the criterion remain unchanged.

#### 2.2.2.2 Temperature Forcing

The temperature forcing was adapted from the Venus' version to include seasonal forcing, with the inclination angle of the rotation axis with the ecliptic plane is around 27°. The vertical profile of the reference temperature for Titan ($T_{ref}$) is given in Table 2.2 [Rannou et al., 2005]. As for Venus, the time scales are less in general than the values obtained in the radiative transfer models. The values for $\tau$ are 8 Earth days, decreasing slightly in the uppermost levels. The vertical temperature perturbation profile, $T_1$(p), is given in Table 2.2, where it was chosen to reflect the peak in absorption of the solar and thermal radiation obtained in McKay et al. [1989].

The temperatures of all points of the GCM grid relax to a zonal averaged temperature profile that depends on the seasonal variations given by the solar declination angle $\delta$ (see Figure 2.3),

$$\delta T_{rad}(\lambda,\phi,p,t) = -\frac{T(\lambda,\phi,p,t) - T_0(\phi,p)}{\tau}\delta t, \tag{2.5}$$

$$T_0(\phi,p) = T_{ref}(p) + T_1(p)(cos(\phi-\delta) - C) \tag{2.6}$$

| | Venus | Titan | Earth |
|---|---|---|---|
| Mean Radius (km) | 6051.8 | 2575.0 | 6371.0 |
| Surface gravity (equator $ms^{-2}$) | 8.87 | 1.35 | 9.78 |
| Bond Albedo | 0.75 | 0.2 | 0.306 |
| Solar Irradiance ($Ws^{-2}$) | 2623.9 | 14.90 | 1367.6 |
| Black-body temperature (K) | 231.7 | 84.5 | 254.3 |
| Sidereal orbit period (days) | 224.701 | (15.95) | 365.256 |
| Tropical orbit period (days) | 224.695 | (15.95) | 365.242 |
| Orbit inclination (deg) | 3.39 | 27 (relative to Saturn) | 0.0 |
| Orbit eccentricity | 0.0067 | 0.029 | 0.0167 |
| Sidereal rotation period (hrs) | (-)5832.5 | 382.68 | 23.9345 |
| (Solar) Length of day (hrs) | 2802.0 | 383.68 | 24.0 |
| Solar day / Sidereal day | 0.480411 | (1.000) | 1.000274 |
| Obliquity of orbit (deg) | 177.36 | | 23.45 |
| Surface Pressure (atm) | 92 | 1.5 | 1 |
| Mean molecular weight (g/mole) | 43.45 | 28 | 28.97 |
| Gas constant (J/K/kg) | 188 | 290 | 287 |
| Specific heat (J/K/kg) | 850.1 | 1005 | 1005 |
| $\kappa$=R/$C_p$ | 0.222 | 0.277 | 0.286 |
| Atmospheric composition | 0.95 $CO_2$ | 0.9-0.97 $N_2$ | 0.78 $N_2$ |
| | 0.035 $N_2$ | | 0.201 $O_2$ |
| Global Super-rotation | 10 | 6-10 | 0.015 |
| Local super-rotation (maximum) | 60 | | 3-8 |
| Sidereal day (Earth days) | 243 | 1.025 | 1 |
| Solar Days (Earth days) | 116.95 | 1.027 | 1.000274 |
| Surface Temperature (approx K) | 730 | 94 | 285 |

Table 2.1: Table from Lee [2006] with the bulk, orbital and atmospheric parameters for Venus [Williams, 2003b], Earth [Williams, 2003a] and Titan (Coustenis and Taylor [1999] and Allison and Travis [1985]).

| Level | Altitude (km) | Pressure (mbar) | $T_{ref}$ (K) | $T_1$ (K) | $\tau$ (Earth Days) | K ($\times 10^8$) |
|---|---|---|---|---|---|---|
| 1 | 0.284 | 1478.2 | 87.388 | 2.000 | 8.0 | 5.00 |
| 2 | 0.727 | 1445.2 | 87.016 | 2.000 | 8.0 | 5.00 |
| 3 | 1.471 | 1391.0 | 86.383 | 2.001 | 8.0 | 5.00 |
| 4 | 2.577 | 1313.6 | 85.489 | 2.002 | 8.0 | 5.00 |
| 5 | 4.077 | 1214.3 | 84.375 | 2.003 | 8.0 | 5.00 |
| 6 | 5.979 | 1097.7 | 83.055 | 2.004 | 8.0 | 5.00 |
| 7 | 8.269 | 970.27 | 81.485 | 2.020 | 8.0 | 5.00 |
| 8 | 10.908 | 839.29 | 79.636 | 2.080 | 8.0 | 5.00 |
| 9 | 13.845 | 711.59 | 77.566 | 2.239 | 8.0 | 5.00 |
| 10 | 17.025 | 592.27 | 75.391 | 2.579 | 8.0 | 5.00 |
| 11 | 20.393 | 484.91 | 73.262 | 3.192 | 8.0 | 5.00 |
| 12 | 23.906 | 391.31 | 71.349 | 4.160 | 8.0 | 5.00 |
| 13 | 27.537 | 311.91 | 69.734 | 5.535 | 8.0 | 5.00 |
| 14 | 31.272 | 245.97 | 68.480 | 7.323 | 8.0 | 5.00 |
| 15 | 35.095 | 192.14 | 67.442 | 9.485 | 8.0 | 5.00 |
| 16 | 38.995 | 148.96 | 66.754 | 11.940 | 8.0 | 5.00 |
| 17 | 42.998 | 114.73 | 67.582 | 14.578 | 8.0 | 5.00 |
| 18 | 47.118 | 87.906 | 67.523 | 17.280 | 8.0 | 5.00 |
| 19 | 51.360 | 67.047 | 68.113 | 19.921 | 8.0 | 5.00 |
| 20 | 55.827 | 50.943 | 70.903 | 22.393 | 8.0 | 5.00 |
| 21 | 60.830 | 38.592 | 77.726 | 24.605 | 8.0 | 5.00 |
| 22 | 66.805 | 29.158 | 86.791 | 26.490 | 8.0 | 5.00 |
| 23 | 73.875 | 21.995 | 95.260 | 28.006 | 8.0 | 5.00 |
| 24 | 81.881 | 16.552 | 102.924 | 29.131 | 8.0 | 5.00 |
| 25 | 90.677 | 12.450 | 109.855 | 29.866 | 8.0 | 5.00 |
| 26 | 100.162 | 9.3499 | 116.128 | 30.227 | 8.0 | 5.00 |
| 27 | 110.284 | 7.0158 | 122.172 | 30.242 | 8.0 | 5.00 |
| 28 | 120.968 | 5.2603 | 128.344 | 29.947 | 8.0 | 5.00 |
| 29 | 132.149 | 3.9415 | 134.718 | 29.384 | 8.0 | 5.00 |
| 30 | 143.760 | 2.9531 | 140.907 | 28.596 | 8.0 | 5.00 |
| 31 | 155.712 | 2.2114 | 146.679 | 27.625 | 8.0 | 5.00 |
| 32 | 167.940 | 1.6552 | 151.769 | 26.513 | 8.0 | 5.00 |
| 33 | 180.391 | 1.2390 | 156.063 | 25.298 | 8.0 | 5.00 |
| 34 | 193.077 | 0.9272 | 159.739 | 24.014 | 8.0 | 5.00 |
| 35 | 205.912 | 0.6940 | 163.357 | 22.680 | 8.0 | 5.00 |
| 36 | 218.888 | 0.5191 | 166.790 | 21.351 | 8.0 | 5.00 |
| 37 | 232.082 | 0.3885 | 169.790 | 20.021 | 8.0 | 5.00 |
| 38 | 245.366 | 0.2907 | 172.881 | 18.715 | 8.0 | 5.00 |
| 39 | 258.856 | 0.2174 | 175.786 | 17.447 | 8.0 | 5.00 |
| 40 | 272.420 | 0.1627 | 178.505 | 16.229 | 8.0 | 5.00 |
| 41 | 286.002 | 0.1218 | 181.239 | 15.067 | 8.0 | 5.00 |
| 42 | 299.541 | 0.0912 | 183.459 | 13.967 | 8.0 | 5.00 |

| Level | Altitude (km) | Pressure (mba) | $T_{ref}$ (K) | $T_1$ (K) | $\tau$ (Earth Days) | K ($\times 10^8$) |
|---|---|---|---|---|---|---|
| 43 | 312.880 | 0.0682 | 185.305 | 12.933 | 8.0 | 5.00 |
| 44 | 325.937 | 0.0510 | 187.973 | 11.965 | 8.0 | 5.00 |
| 45 | 338.567 | 0.0382 | 189.673 | 11.064 | 8.0 | 5.00 |
| 46 | 350.661 | 0.0286 | 194.856 | 10.228 | 8.0 | 5.00 |
| 47 | 362.193 | 0.0213 | 199.583 | 9.457 | 8.0 | 5.00 |
| 48 | 373.081 | 0.0160 | 202.780 | 8.747 | 8.0 | 5.10 |
| 49 | 383.502 | 0.0119 | 203.597 | 8.096 | 8.0 | 5.15 |
| 50 | 393.495 | 0.0088 | 201.680 | 7.500 | 8.0 | 5.30 |
| 51 | 403.864 | 0.0062 | 197.001 | 6.957 | 8.0 | 5.60 |
| 52 | 415.523 | 0.0041 | 190.870 | 6.463 | 8.0 | 6.00 |
| 53 | 439.416 | 0.0020 | 183.070 | 6.014 | 6.0 | 6.50 |
| 54 | 512.468 | 0.0004 | 186.165 | 5.607 | 5.0 | 7.00 |

Table 2.2: Values used in the Titan GCM.

where C is equal to $\frac{\pi \cos\delta}{4}$, which is the result of forcing the integral of cos($\phi - \delta$) - C to be zero over the domain, and $\delta$ is the solar declination angle. The values for $\delta$ are simplified, they are assumed to vary sinusoidally between the maximum value 27° and the minimum -27°.

### 2.2.3 Results

In this subsection we show preliminary results of Titan's model, which was integrated for 34000 Earth days. The atmosphere started from a rest state and relaxed to a statistically steady state. The "spin-up" phase of the model integration is analysed from the evolution of the global kinetic energy of the atmosphere,

$$E_k = \int\int\int (u^2 + v^2 + w^2)\frac{a^2 cos(\phi)}{g} d\phi d\lambda dp \tag{2.7}$$

where $u$, $v$ and $w$ are the three components of the wind field, $a$ is the Earth bulk radius, $\phi$ is the latitude, $\lambda$ is the longitude and $p$ is the pressure. Figure 2.4 shows the integrated kinetic energy where the energy associated with $w$ was neglected. This Figure shows a fast "spin-up" phase where oscillations around a roughly mean value that is constant during the time are visible. The oscillations are due to the seasonal forcing in the thermal relaxation scheme that affects the vertical transport of angular momentum in the stratosphere. During most part of the year on Titan, the Hadley cell extends from pole-to-pole, where the symmetric two-cell configuration seems to appear in a limited transition period in the equinoxes. It is in this period, between the equinox and solstice, that the maximum of angular momentum in the stratosphere is reached.

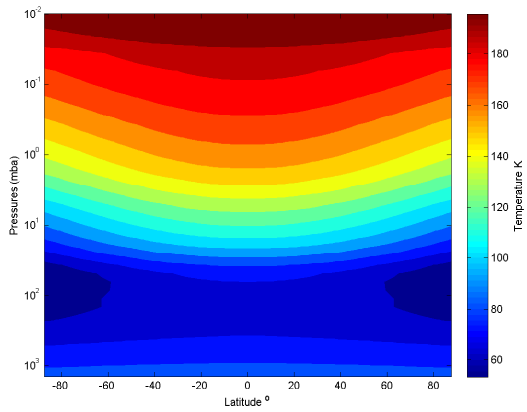


(a) Zonal averaged temperature field ($\delta = 0$)

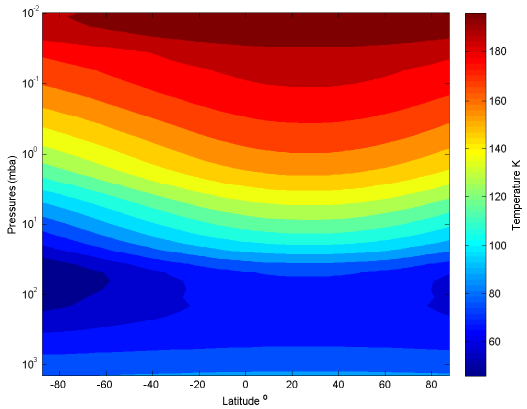


(b) Zonal averaged temperature field ($\delta = 27$)

Figure 2.3: Zonal temperature fields ($T_0$) for two different declination angles, **a** $\delta = 0$ (one equinox) and **b** $\delta = 27$ (North summer solstice).

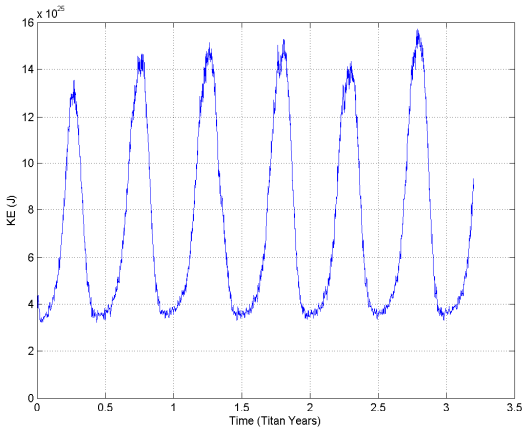


Figure 2.4: The globally integrated kinetic energy from the simulated atmosphere of Titan. The vertical component $w$ was neglected in this integration.

Figure 2.5 shows the zonal winds in three distinct seasons. In the solstices we observe stronger jets in the winter hemisphere, which are produced in the downward branch of the non-asymmetric pole-to-pole Hadley cell. In the equinox the zonal winds pattern tend to be symmetric in relation to the equator. The position of the jets produced in the solstices are in agreement with the model's results from Hourdin et al. [1995], but their magnitudes are lower.

The results need to be studied in more detail for a better understanding of the super-rotation phenomenon which is thought to follow the GRW mechanism in Titan (chapter 1), and other important global atmospheric phenomena related with the fast rotation of the atmosphere. Some important studies are needed such as: diagnostic computations of eddy statistics and model climatology.

The simplicity of the parameterizations requires the fine tuning of some variables to improve the results of the SGCM. The function $T_p$ from the thermal forcing scheme and the horizontal diffusion in the model need a special attention since the model is very sensitive to changes of their shape (Lee [2006]), and a sensitivity study is also needed to better constrain them.

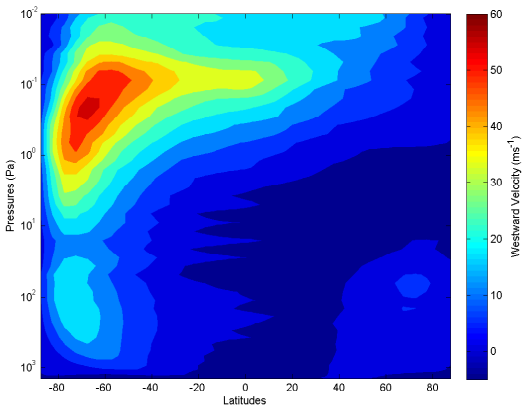


(a) North Summer

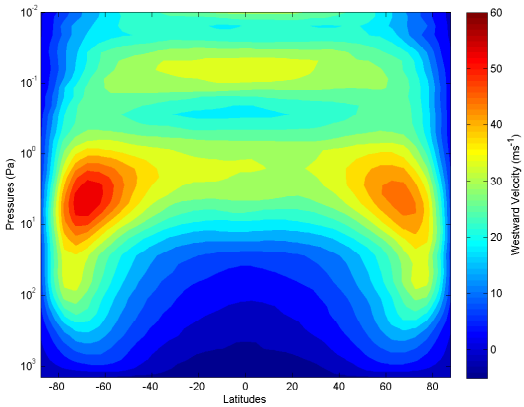


(b) North Spring

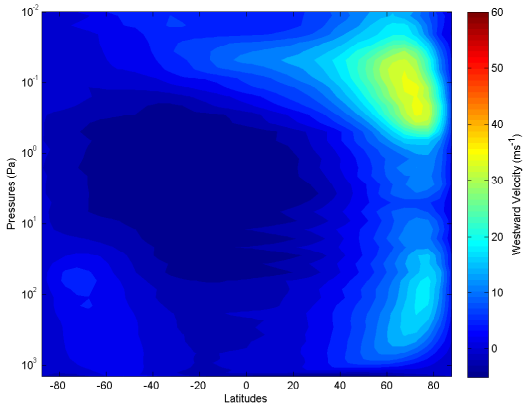


(c) Southern Summer

Figure 2.5: Zonal winds obtained from Titan SGCM for three different seasons.

CHAPTER 3

# Zonal Winds on Venus

## Contents



On Earth, which is a relatively rapidly rotating planet (with small zonal Rossby number), the geostrophic approximation is often assumed for large-scale atmospheric motions, where the pressure gradient term is approximately balanced by the Coriolis term. In the mesosphere of Venus, this approximation fails because in those layers of the atmosphere we have strong winds overlying a slowly rotating planet. In this case, the cyclostrophic approximation in which the centrifugal term balances the geopotential gradient term, may be used. From the meridional component of the equation of motion in a planetary atmosphere, we can obtain the thermal wind equation from the balance of these two terms,

$$\frac{u^2 \tan\phi}{a} = -\frac{1}{a}\frac{\partial \Phi}{\partial \phi}, \tag{3.1}$$

where $\phi$ is latitude, $u$ the zonal wind, $a$ the radius of the planet, $p$ the pressure, $\rho$ the density and $\omega$ the rotation rate of the planet. This equation can be simply written as a function of the temperature fields, assuming that we have an ideal gas. Recent results of the zonal thermal winds obtained in a cyclostrophic regime are consistent with the cloud tracking results at mid-latitudes, but inconsistent in the polar region where the values obtained are less than or close to zero (Piccialli et al. [2008], Figure 3.1). In observations from Piccioni et al. [2007] it is possible to see the clear rotation of the double vortex in the same direction of the global mean zonal wind.

In the present investigation we have studied the full zonally averaged meridional component of the equation of motion, in which we have analysed the contributions of different terms from the GCM's results. The aim was to clarify the real nature of the atmosphere's zonal mean dynamics, especially at high latitudes where the integration of the thermal wind equation to retrieve the zonal winds seem to breakdown (Newman et al. [1984] and Piccialli et al. [2008]). We also explore the sensitivity of the upward integration of the thermal wind equation to different choices of lower boundary conditions and propose a method to reduce the problems regarding this constraint. The method to retrieve the zonal thermal winds in

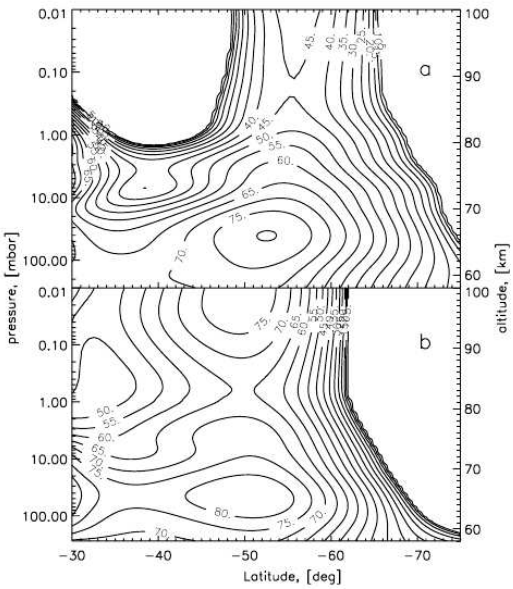


Figure 3.1: The two images show the contours of the zonal thermal wind speed (m/s) for two different local times: the top one is 18:00-20:00 and the other 03:00-05:00. These contours were obtained by Piccialli et al. [2008] assuming the cyclostrophic approximation at the mesosphere in Venus. The VIRTIS temperature retrivals were used.

Venus has been shown to be a very powerful tool to study the dynamics of the atmosphere, due to the large number of temperature retrievals obtained from Venus Express data.

The Venus Simplified General Circulation Model (SGCM) used obtains a realistic and dynamically self-consistent representation of the circulation of the Venus' atmosphere (Lee [2006] and Lee et al. [2007]) and its results were used as a guide to improve the zonal thermal winds retrieved from the VIRTIS temperature maps (Grassi et al. [2010]).

### 3.0.4 Model

The Oxford Venus SGCM has been used to study and characterise zonal winds in the Venus' atmosphere. A reference simulation used for the present study was integrated for $4.1\times10^4$ (Earth) days, with a time-step of 10 minutes and did not include a diurnal cycle or surface topography. The numerical model integration started with the atmosphere at rest with the underlying planet, a surface pressure of 92.0 bar and a vertical temperature profile very close to the VIRA (Venus International Reference Atmosphere) model for each grid point. Fig. 3.2 shows meridional cross-sections of the zonal winds and a temperature map that were zonally and time averaged in the last hour of the simulation. The atmospheric circulation is close to being statistically steady, although it does exhibit a slight increasing tendency in the kinetic energy of the global atmosphere even after more then 100 Earth years of spin-up.

The zonal winds produced by the model are illustrated in Fig. 3.2(a) for the Northern hemisphere (the pattern is similar to the Southern hemisphere). A jet structure is seen to

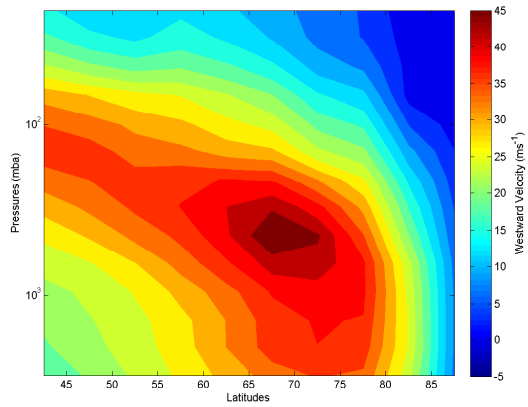


(a) (prograde) Westward Velocity (m/s)

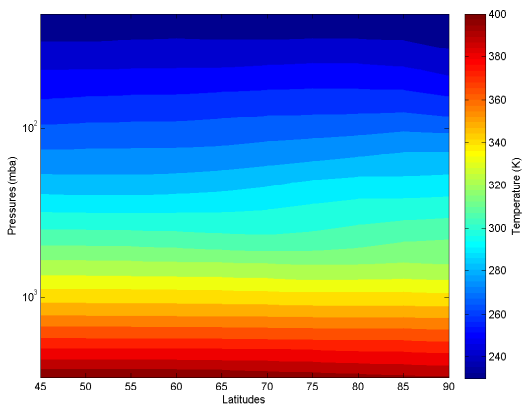


(b) Temperatures (K)

Figure 3.2: Zonally and time (one hour) averaged maps calculated by the SGCM, at the end of the model's integration in the North Hemisphere: (**a**) zonal winds ($\mathrm{m\,s^{-1}}$); (**b**) temperature map (K).

form at roughly 2 bar and $65^o$ N latitude with a magnitude of around 45 $\mathrm{m\,s^{-1}}$ (about a half of the wind strength observed by eg. Schubert 1983). The zonal wind speed in the equatorial mesosphere region is slower than in the mid-latitudes but it is still prograde and super-rotating with respect to the solid planet.

The temperature map (Figure 3.2(b)) shows two different gradients of temperature towards the pole: near the bottom of the jet (negative gradient) and near the top (positive gradient). Using a temperature anomaly map it is possible to observe in the polar regions (around $75^o$ N latitude) of the atmosphere between 1 bar and 5 bar, colder temperatures than in the poles and in the equator, which is known as the cold collar phenomenon. The warm pole and the polar cold collar temperature structure are observed in the Venus atmosphere (Taylor et al. [1979]), despite the magnitudes of the anomalies being lower in the model.

### 3.0.5 Zonally averaged meridional component of the equation of motion

The full zonally averaged meridional component of the equation of motion on a spherical planet of radius $a$ and angular velocity $\Omega$, is used in this work to study the contribution of each term. The equations are defined using an Eulerian-mean, fixing latitude $\phi$, time $t$ and altitude $z$, for each term of the equations,

$$\bar{u}[\bar{u}a^{-1}\tan\phi+f]+a^{-1}\bar{\Phi}_{\phi} = -(a\cos\phi)^{-1}(\overline{v'^2}\cos\phi)_{\phi}-\overline{u'^2}a^{-1}\tan\phi-Residual, \quad (3.2)$$

where the subscript means a partial derivative, and the quadratic functions of disturbance variables, which were written on the right side of the equation, are the "rectified eddy-forcing" terms [Andrews et al., 1987]. The functions of disturbance variables of lower order were neglected. The eddy terms measure the interaction of the mean flow with superimposed disturbances, that can have a very important effect on the zonal mean circulation. The residual term quantifies the remaining terms that we are neglecting in this approximation.

In Figure 3.3, the results show that the equation is dominated mainly by two terms: the centrifugal acceleration and the geopotential gradient. The two eddy terms do not have negligible magnitude in the polar region and seem to be related to the turbulent zone near the jets, leading to a breakdown of the cyclostrophic approximation. The residual does not have negligible values in the polar region and becomes more relevant for higher altitudes above the jet. It includes all the terms that we are neglecting and seems to be more relevant in the turbulent regions. Another possibility why the residual is not completely negligible at high latitudes maybe related to the CFL's (Courant-Friedrich-Lewi) condition, that filters any zonal winds which are too fast compared with the wind speeds for that latitude orientation in the polar region.

A latitude-pressure map of the two main eddy terms for this case are shown in Fig. 3.4. Both terms have important contributions at high latitudes, stronger in the jet region (around 2 bar), and apparently leading to a partial breakdown of the cyclostrophic balance. In Fig. 3.3, we can see that the eddy terms can have a larger magnitude than the zonal mean cyclostrophic terms for latitudes higher than $80^o$.

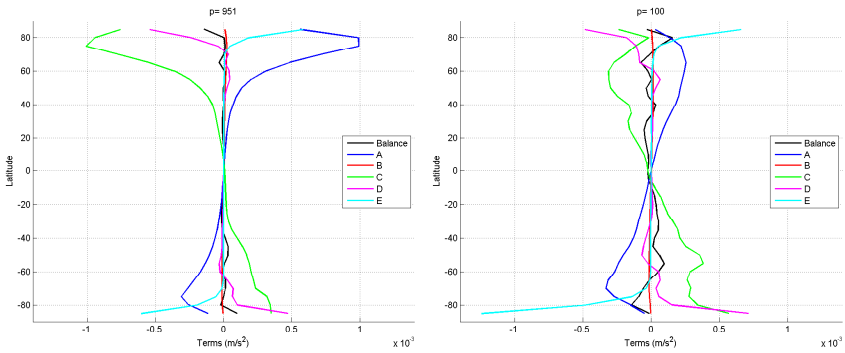


(a) Evaluation at 951 hPa. (b) Evaluation at 100 hPa.

Figure 3.3: The different lines represent each term of the meridional component of the equation of motion. They were obtained after $4.1\times10^5$ earth days in the SGCM integration without diurnal forcing. Each term was averaged over longitude and time (1 hour). Note: $A = \frac{u^2 \tan\phi}{a}$, $B = u2\Omega sin\phi$, $D = \frac{1}{a}\frac{\partial\Phi}{\partial\phi}$, $C = (a\cos\phi)^{-1}(\overline{v'^2}\cos\phi)_\phi$ and $D = \overline{u'^2}a^{-1}\tan\phi$; where $\phi$ is the latitude and $\Omega$ is the rotation rate of the planet.

### 3.0.6 Zonal thermal winds

The zonal thermal wind equation applied to the Venus mesosphere is the balance of two terms, the centrifugal and geopotential gradient terms, as explained in the introduction. Following Newman et al. [1984] and Piccialli et al. [2008] we used the upward-integration of the thermal wind equation in the form of,

$$2u\frac{\partial u}{\partial\zeta} = -\frac{R}{tan\phi}\frac{\partial T}{\partial\phi}|_{p=const}, \tag{3.3}$$

where $R$ is the gas constant and $T$ the temperature. The variable $\zeta$ is definedas $-log(\frac{p}{p_o})$, where $p$ is the pressure at each altitude level and $p_o$ is a reference pressure. Figure 3.6(a) shows the thermal zonal winds that were retrieved from the temperature map (Figure 3.2(b)) obtained by the SGCM for Venus and using for the lower boundary condition the zonal winds values obtained from the same model.

The new zonal winds obtained are very similar to the model's zonal winds, the main differences appear in the polar region between 300 hPa and the top, where as seen in the previous subsection, the cyclostrophic balance breaks down due to the significant contribution of the two main eddy terms and non-negligible residuals in this region. Figure 3.6(b) shows the thermal zonal winds obtained using as lower boundary condition:

$$u_0 = 100 \times (sech(\frac{\phi - 85^o}{15^o}) + 15) \times cos(\phi). \tag{3.4}$$

The main difference between this result and the previous one is the decrease in magnitude of the winds in the polar region and in the jet. As would be expected, the use of an inappropriate lower boundary condition produces incorrect results. Figure 3.5 shows the variability

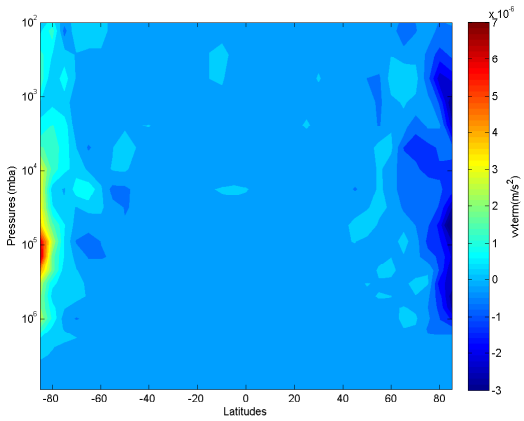


(a) Eddy forcing term: $(a\cos\phi)^{-1}(\overline{v'^2}\cos\phi)_\phi$

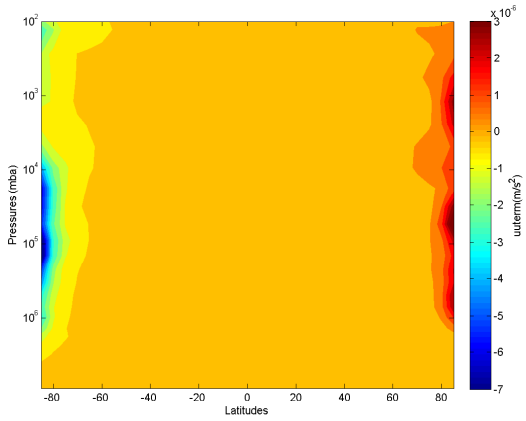


(b) Eddy forcing term: $\overline{u'^2}a^{-1}\tan\phi$

Figure 3.4: Eddy terms obtained from the equation 3.2. The derivation of these terms are explained in Andrews et al. [1987].

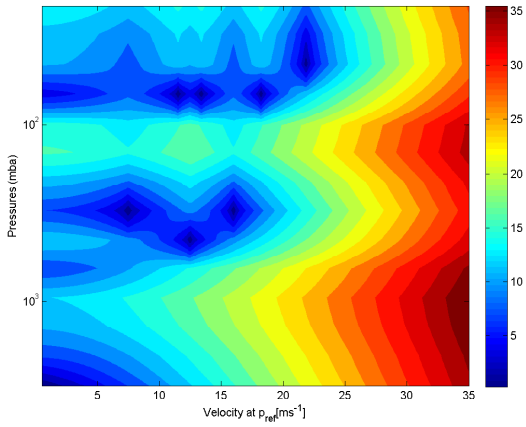


Figure 3.5: Variability of the zonal winds for different values of lower boundary condition at a fixed latitude ($82^o$).

of the zonal winds with altitude at a high latitude ($82^o$) for a range of lower boundary conditions. The retrieval of the zonal winds on this region where the eddy terms are important would require a new method based on cyclostrophic balance and an eddy diffusion parameterisation (eg. **?**). We have already tested some possible methods but without success, using the relative vorticity gradient or potential vorticity as a base for the eddy diffusion parameterisation.

The upward-integration is sensitive to changes in the polar region lower boundary condition as shown in Figures 3.10 and 3.5. This difficulty can largely affect the results. A method that was explored to reduce this sensitivity consists in integrating the thermal wind equation downward in altitude assuming a solid body rotation at the top. This integration is applied in a latitude region starting from the position of the jet, up to the pole (Figure 3.7). The imposition of a mean atmospheric vortex in the Venus mesosphere associated with an approximated solid body rotation circulation, is plausible for the following reasons: The flow cannot be angular momentum conserving up to the pole, otherwise the zonal winds would be unrealistic, increasing with the inverse of the cosine; The barotropic eddies associated with the jet in the Venus atmosphere tend to mix towards a state of approximate uniform vorticity (**?**). Flow polewards of mid-latitudes jet is baratropically unstable. Solid body rotation regime is uniform $\xi(r)$ in cylindrical polar coordinates and approximate to a slowly varying $\xi(\theta)$ in spherical polar coordinates near the pole ($\xi$ is vorticity, $r$ is the radial coordinate and $\theta$ the latitude). On the observational side, a solid body rotation is in line with the zonal winds most commonly obtained by the SGCM in the polar region for altitudes above the jet, broadly similar to the approximate Rankine vortex observed in Venus (**?**).

The new method, in general, increases the magnitude of the winds at high latitudes, improving the previous results. The new zonal winds were obtained from a better estimate of the lower boundary condition (new method). This method can be important since lower boundary condition has been estimated from cloud tracking methods, which are often not very accurate at high latitudes because of a lack of clearly defined features in cloud images.

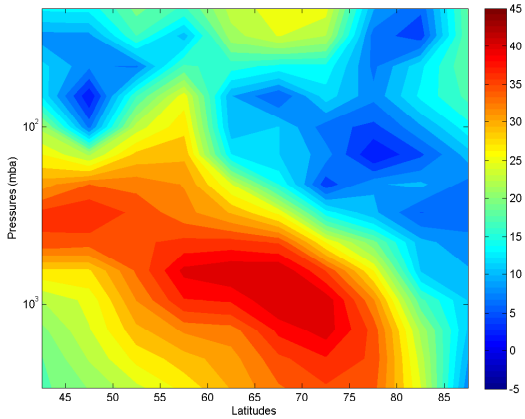


(a) Thermal zonal winds obtained from the true lower boundary condition.

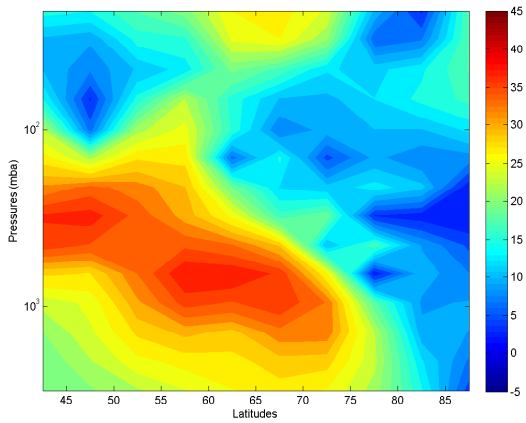


(b) Thermal zonal winds obtained from a hypothetical lower boundary condition.

Figure 3.6: Thermal zonal winds obtained with different lower boundary conditions. For Figure (**a**), was used the zonal winds values obtained by the model and for (**b**) the values obtained from the equation 3.4.

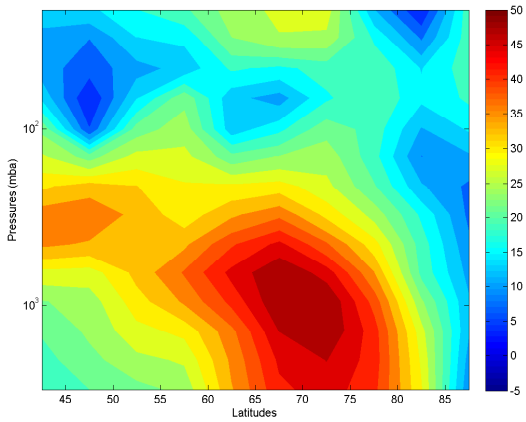


Figure 3.7: Thermal Zonal winds obtained applying the new method to improve the values in the polar region.

### 3.0.7 Using Observational Data

In this section we study the thermal zonal winds obtained from the latitude-pressure mesosphere temperature map for a local time, retrieved by the mapping IR channel of the Visual and Infrared Thermal Imaging Spectrometer (VIRTIS-M) on board the Venus Express spacecraft.

#### 3.0.7.1 Temperature Field

The latitude-pressure temperature map used is part of the compilation of temperature retrievals from Grassi et al. [2010]. The map covers 1-100 hPa from 45$^o$ latitude up to the pole in the southern hemisphere. The overall error in the retrieved temperature in this region does not exceed 4 K and is very accurate between 7 and 70 hPa. The map of Temperatures is shown in Figure 3.8, where is possible to observe the cold collar at 65$^o$S and the temperatures increasing monotonically towards the pole above 12.6 hPa.

#### 3.0.7.2 Zonal Thermal Winds

The thermal zonal winds were obtained using equation 3.3. The upward-integration was done using the method described in the previous section applied to the temperature map from the SGCM. The lower boundary condition at 100 hPa was Piccialli et al. [2008],

$$u_0 = 45 \times (sech(\frac{\phi - 56}{9}) + 75) \times cos(\phi). \tag{3.5}$$

For each level the latitudinal profile of the temperature was fitted to a polynomial of degree 5 in order to smooth the data and facilitate the evaluation of $[dT/d\phi]_{p=const}$. Figure 3.10(a) shows the thermal zonal winds obtained from the VIRTIS data, with a jet reaching a maximum of -80 $m/s$ at a latitude of -50$^o$. As was observed in other studies, the zonal winds in the polar region are weaker than would be expected from observations of the polar vortex. In the work of Limaye [1985] it is possible to have an idea of the zonal winds in the

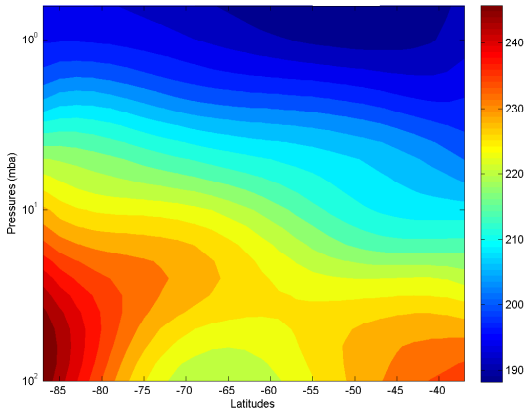


Figure 3.8: Temperature map for 2400 LT derived from VIRTIS temperature retrievals (Grassi et al. [2010].

problematic region. He used a method that obtains the zonal winds using the cyclostrophic approximation but from the meridional slope of the pressure surfaces (Figure 3.9). This method has the advantage of not requiring an integration, avoiding the problems with the choice of the lower boundary condition. A problem with this procedure is the difficulty in obtaining the observational data required; however the results obtained show stronger zonal winds in the polar region.

Following the study from the SGCM results we used the method suggested to reduce the problems in the polar region (Figure 3.10(b)). This method, which better estimates the lower boundary condition, increases the zonal winds in the region where it is applied to (for all altitudes and from the latitude position of the jet up to the pole). The results for this case are in better agreement with the ones in Limaye [1985] and with the expected values for this region (non-negligible winds in the westward direction).

This work needs to be validated with more observational data and with other methods that retrieve the zonal winds in the polar region. However, the main difficulties in assuming the cyclostrophic approximation from the SGCM studies were pointed out, which can lead us to an improved retrieval method.

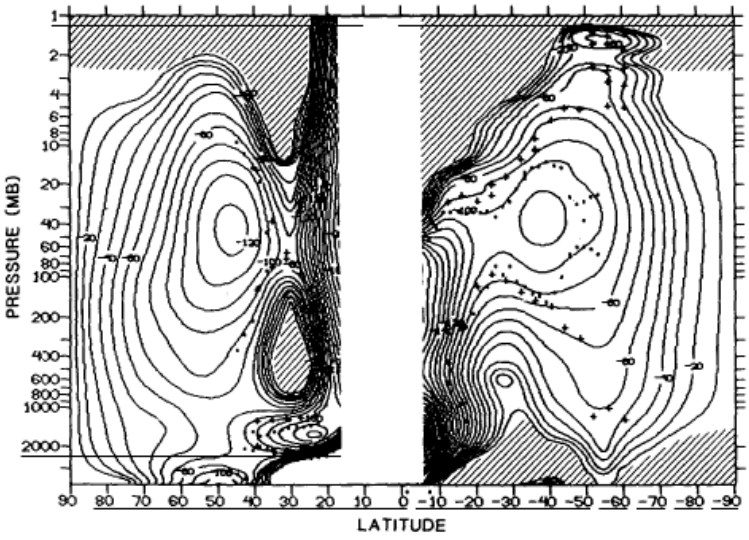


Figure 3.9: Zonal wind derived from the cyclostrophic approximation and the meridional gradient of the height of the isobaric surfaces (Limaye [1985]).

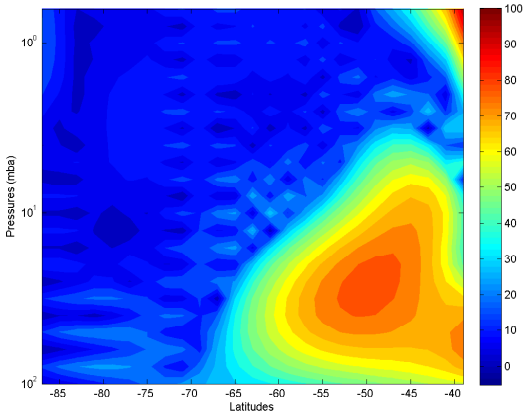


(a) Thermal zonal winds obtained from the equation for the lower boundary condition.

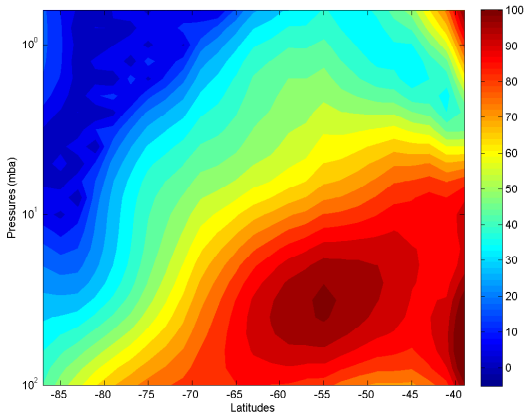


(b) Thermal zonal winds obtained from the new method.

Figure 3.10: Zonal thermal wind speed (m/s) for 2400 LT derived from VIRTIS temperature retrievals (Grassi et al. [2010]) assuming cyclostrophic balance. Figure (**b**), uses the new method to better estimate the lower boundary condition and (**a**) is from equation 3.5.

CHAPTER 4

# New Radiation Scheme in Venus GCM

## Contents



The current Oxford Simplified General Circulation Model (SGCM) applied to the atmosphere of Venus uses a linearized temperature forcing scheme to simulate the radiative heating/cooling of the atmosphere (Lee et al. [2007]). This simple parameterisation does not have a real basis on radiative transfer formulations, which induces inaccuracies in the computation of heating/cooling rates. We are adapting and extending this 3D time-dependent numerical circulation model of the atmosphere to include a new physically-based radiative transfer formulation. This new parameterisation uses different approaches in the two main wavelength bands: solar radiation (0.1-5.5$\mu$m) and thermal radiation (1.7-250$\mu$m).

## 4.1 New Solar Radiation Scheme

The lack of a solar radiation code within the Venus climate modelling community motivated us to develop a fast, flexible and accurate new formulation to compute the heating rates over the Venus's Atmosphere. The method used is a combination of $\delta$-Eddington, adding-layer and correlated k-distribution methods. The important active components that interact with the solar radiation were taken into account. The model uses the absorption and

scattering of 3 different gases ($CO_2$, $SO_2$ and $H_2O$), 4 size categories of $H_2SO_4$ aerosols, an unidentified UV absorber and the Rayleigh scattering of $CO_2$ and $N_2$. The model's results are compared with a more accurate method by Crisp [1986], who calibrated his results with measurements from Solar Flux Radiometer experiments obtained by the Pioneer Venus mission (Moroz et al. [1985]).

### 4.1.1 Introduction

The portion of the atmosphere explored in the GCM covers the region between the surface and 100 km altitude. The main solar radiative processes in the Venus atmosphere occur in the mesosphere (between 100 and 55 km altitude) which accounts for the important contribution of the cloud deck that reflects 75% of the incident sunlight. A large amount of solar energy is absorbed within the cloud where an unidentified substance is responsible for the absorption of the UV radiation in the upper clouds, causing remarkable features in the UV images of the atmosphere (Figure 4.2). Above the cloud top the $CO_2$ absorption dominates. In the deepest atmosphere the absorption of the 3 gases (the mass mixing ratio of H2O and SO2 increases) becomes important as well as the Rayleigh scattering, but producing very small heating rates in comparison with the rest of the atmosphere (up to 3 orders of magnitude lower). The estimate for the solar energy absorbed at the surface averaged over the planet is around 2.5% of the total incident solar energy (Tomasko et al. [1980] and Figure 4.1).

The differential absorption of the sunlight by the atmosphere has a key role driving the circulation of the atmosphere and in maintaining the thermal structure. The thermal tides are thought to be an important mechanism to maintain the equatorial super-rotation of the atmosphere (Newman and Leovy [1992] and Lebonnois et al. [2010b]), which increases the importance of having a self-consistent parameterisation for the solar radiation in the Venus GCM.

In the next subsection, we describe the optical properties of the Venus atmosphere which includes the distribution and composition of the different gases and the aerosols. This is followed by the subsections about the code's structure, with all the explanations for the approximations used. Finally, in subsection 4.1.4.4 the results are discussed.

### 4.1.2 Optical Properties of the Venus Atmosphere for Solar Radiation

#### 4.1.2.1 Gases

The optical properties were computed for the 3 principal gases that interact with the solar radiation in the Venus atmosphere: carbon dioxide ($CO_2$), water ($H_2O$) and sulfur dioxide ($SO_2$). Figure 4.3 shows the volume mixing ratios for these 3 gases. The three profiles were taken from the VIRA model (**V**enus **I**nternational **R**eference **A**tmosphere). The Venus atmosphere is composed mainly of $CO_2$ (assumed to be well mixed in the atmosphere, 0.96 vmr). The coefficients of absorption used for $CO_2$ and $H_2O$ were compiled in the work of Lee et al. [2010a]. These coefficients were computed using parameters from the HITRAN 2004 database (Rothman et al. [2005]) and the HITEMP $CO_2$ (Rothman et al. [1995]) and stored using a K-distribution method (Lacis and Oinas [1991]). The K-tables

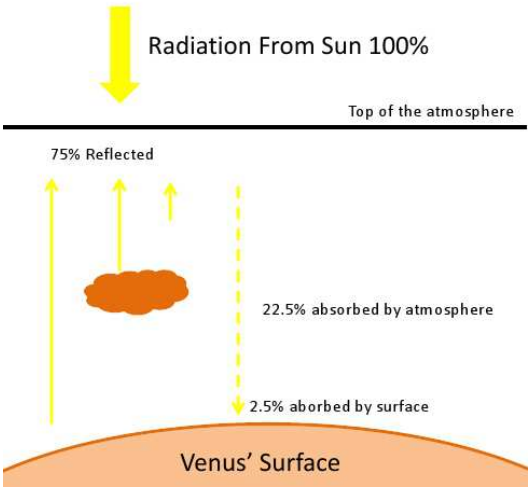


Figure 4.1: The different components of the radiative energy budgets in Venus.

were calculated by Lee and Richardson [2010] on a 0.1 micron resolution grid between 0.1 and 50.1$\mu$m, for 20 reference pressures between 0.1Pa and 14MPa (equally spaced in a log scale), 20 reference temperatures from 150K to 1100 (equally separated spaced) and 20 Gaussian ordinates (spectral fractions). Self-broadening was assumed when calculating the $CO_2$ opacity and air-broadened for $H_2O$ (deuterium enriched). The coefficient of absorption for each model level was obtained by interpolating the K-table linearly (in log scale for pressure) for the required temperature and pressure. The coefficients of absorption for $SO_2$ were obtained from a table available in Crisp [1986].

#### 4.1.2.2 Aerosols

The main cloud deck is composed mostly of sulphur dioxide and sulphuric acid droplets and it extends from about 45 to 65 km above the surface, with haze layers above and below. In the ultraviolet (UV), visible and most of the infrared wavelength range, the clouds are very thick, hiding completely the surface of the planet. The clouds have particles of three different modes whose proportions are different for different layers, with sizes ranging from less than 1 to over 30 $\mu m$ in diameter. The smallest particles, 'mode 1' droplets, extend throughout the top of the clouds and their composition is still unknown. The droplets of 'mode 2' are mainly $H_2SO_4$ and $H_2O$, and the ones of 'mode 3' are probably composed of "bigger droplets" of $H_2SO_4$ and are located in the lower and mid cloud layers. The clouds have a very high optical depth and a high single scattering albedo in some of the most significant spectral intervals, but they are not completely opaque at all wavelengths: some visible and near-IR spectral windows can be observed. From the near-IR mapping spectrometer (see Figure 4.4), it is possible to observe variability in the horizontal and vertical structure of the clouds, which is a consequence of the dynamical transport, production and destruction of particles in the clouds.

The cloud model used in this work was adapted from Crisp [1986], where the number

| | Mode 1 and UV absorber | Mode 2 | Mode 2' | Mode 3 |
|---|---|---|---|---|
| Effective radius ($\mu$m) | 0.49 | 1.18 | 1.40 | 3.65 |
| Effective variance ($\mu$m) | 0.22 | 0.07 | 1.23 | 1.30 |

Table 4.1: Microphysical properties of the aerosols. Mode 2 is divided into submodes 2‘ and 2, that corresponds to different regions in the clouds (lower/middle clouds and upper clouds respectively).

density (equatorial cloud model) was interpolated for our model's vertical resolution and the scattering and extinction efficiencies interpolated for $0.1\mu$m resolution. The composition of the clouds is assumed to be $75\%$ sulphuric acid and $25\%$ water. The microphysical properties used for each mode (1, 2, 2',3 and UV absorber) are listed in Table 4.1.

The UV absorber in the mesosphere is simulated assuming that the distribution of this "artificial" constituent is the same as the mode 1 particles between 56.5 km and 71 km. The empirical absorption between 0.3 and 0.7 $\mu$m is tuned until the spectral dependence of the spherical albedo matches the observations (Crisp [1986]). Outside this spectral region the absorption is set to zero.

The computation of the optical depth for each particle mode was done using a rescaling method,

$$\tau_x(\lambda) = \frac{Q_x(\lambda)}{Q_{ext}(0.63\mu m)}\tau_{ext}(0.63\mu m), \tag{4.1}$$

where $\tau_{ext}(0.63\mu m)$ and $Q_{ext}(0.63\mu m)$ are the extinction optical depth and efficiency at 0.63 $\mu$m and the symbol $x$ identifies the variable with extinction, absorption or scattering properties. The values of $\tau_{ext}(0.63\mu)$ were determined by the study of observational experiments onboard the Pioneer Venus satellite (Crisp [1986]).

### 4.1.3 Rayleigh scattering

We implemented in the solar radiation code a Rayleigh scattering effect due to the presence of $CO_2$ and $N_2$ molecules in the Venus atmosphere. According to Hansen and Travis [1974], the scattering coefficient per unit length for anisotropic gaseous molecules in random orientation is,

$$k_{sca} = \frac{8\pi^3}{3}\frac{(n_g^2-1)^2}{\lambda^4 N}\frac{6+3\delta}{6-7\delta} \tag{4.2}$$

where $\delta$ is the anisotropy factor, $N$ is the number of molecules per unit volume and $n_g$ is the refractive index. The values of $n_g$ for $CO_2$ and $N_2$ were obtained for different pressures ($P$) and temperatures ($T$),

$$n_g = 1 + \frac{\beta \times 10^{-6}(P/P_0)}{(1-\alpha T)(\mu - \lambda^{-2})} \tag{4.3}$$

where $P_0$ is a reference pressure (1.01325 bars), $\lambda$ is the wavelength and $\beta$, $\mu$ and $\alpha$ are

| Constant | $CO_2$ | $N_2$ |
|---|---|---|
| $\mu$ | 169.94 $\mu m^{-2}$ | 156.63 $\mu m^{-2}$ |
| $\beta$ | 55939 | 69049 |
| $\frac{1}{\alpha}$ | 273 K | 269.1 K |

Table 4.2: Empirically-determined constants form Washburn.

empirically derived constants from Washburn(Table 4.2). The values of $\delta$ are 0.0305 for $N_2$ and 0.0805 for $CO_2$.

### 4.1.4 The Solar Radiative Transfer Model

The two-stream solar radiation code is a combination of three methods: delta-eddington approximation, k-distribution and a layer-adding method. The atmosphere is divided into 37 horizontally and vertically homogeneous layers. The assumed homogeneity of the layers means that the physical properties in each layer are constant. An extra layer was included to avoid excessive heating in the top model's layer, when the top pressure is not very low (Briegleb [1992]).

The computation of the solar heating rates in each layer is associated with divergence of the spectral-integrated net radiative flux and to a specific heat at constant pressure. The variation of $C_p$ (Jkg$^{-1}$K$^{-1}$) with pressure is assumed to be the following,

$$C_p = 443.15 + 1.688T - 1.269 \times 10^{-3}T^2 + 3.47 \times 10^{-7}T^3. \tag{4.4}$$

The equation is a least-square fit to laboratory measurements for a pure $CO_2$ atmosphere, which was used by Crisp [1986].

The solar spectrum was divided into 55 bands from 0.1 to 5.5$\mu$. The solar fluxes at the top of the atmosphere were based on the results presented in the MODTRAN 3.7 program (Liou [2002]) and converted using 0.7 AU for the mean distance Venus-Sun.

#### 4.1.4.1 Two-Streams with $\delta$-Eddington Solution

A numerical solution based on the two-stream method was used to simplify the radiative transfer equation that becomes difficult to solve when the particle scattering is included. This method divides the radiance into an upward and downward component.

For each model's layer the monochromatic optical properties were defined taking into account the several absorbers and/or scatters constituents,

$$\tau = \sum_i \tau_i, \tag{4.5a}$$

$$w = \frac{\sum_i w_i \tau_i}{\tau}, \tag{4.5b}$$

$$g = \frac{\sum_i g_i w_i \tau_i}{w\tau}, \tag{4.5c}$$

$$f = \frac{\sum_i f_i w_i \tau_i}{w\tau}. \tag{4.5d}$$

These equations define the extinction optical depth $\tau$, the single-scattering albedo $w$, the asymmetry parameter $g$ and the forward scattering fraction $f$ for each homogeneous layer.

The simple two-stream method does not produce accurate results when significant absorption is involved such as in the aerosols region in the Venus' atmosphere. This problem is due to the fact that the scattering by particles present in the atmosphere is highly peaked in the forward direction. A simple approach to avoid this difficulty is to use a $\delta$ adjustment to the radiative parameters. The method used in this work is called the $\delta$-Eddington approximation. The radiative parameters are scaled removing the fraction of scattered energy related to the forward peak. This approximation incorporates in a simple formulation the multiple scattering phenomena in the atmosphere. The scaled parameters are defined as,

$$\tau^\star = \tau(1 - wf), \tag{4.6a}$$

$$w^\star = w(\frac{1-f}{1-wf}), \tag{4.6b}$$

$$g^\star = \frac{g-f}{1-f}. \tag{4.6c}$$

The radiation was divided in direct and diffuse components. The reflectivity and transmissivity were computed for each layer, following the equations (nonconservative solutions, w < 1),

$$R(\mu_0) = (\alpha - \gamma)\bar{T}e^{-\frac{\tau^\star}{\mu_0}} + (\alpha + \gamma)\bar{R} - (\alpha - \gamma), \tag{4.7a}$$

$$T(\mu_0) = (\alpha - \gamma)\bar{R}e^{-\frac{\tau^\star}{\mu_0}} + (\alpha + \gamma)\bar{T} - (\alpha + \gamma - 1)e^{-\frac{\tau^\star}{\mu_0}} \tag{4.7b}$$

$$\bar{R} = (u+1)(u-1)(e^{\lambda\tau^\star} - e^{-\lambda\tau^\star})N^{-1} \tag{4.7c}$$

$$\bar{T} = 4uN^{-1} \tag{4.7d}$$

where $\alpha, \gamma, \lambda$, N and u are defined as,

$$\alpha = \frac{3}{4}w^\star\mu_0\frac{1 + g^\star(1 - w^\star)}{1 - \lambda^2\mu_o^2} \tag{4.8a}$$

$$\gamma = \frac{1}{2}w^\star\frac{1 + 3g^\star(1 - w^\star)\mu_0^2}{1 - \lambda^2\mu_0^2} \tag{4.8b}$$

$$N = (u+1)^2e^{\lambda\tau^\star} - (u-1)^2e^{-\lambda\tau^\star} \tag{4.8c}$$

$$u = \frac{3}{2}\frac{1 - w^\star g^\star}{\lambda} \tag{4.8d}$$

$$\lambda = \sqrt{3(1 - w^\star)(1 - w^\star g^\star} \tag{4.8e}$$

The notation used is the same as Coakley et al. [1983] and Briegleb [1992]. $R$ and $T$ are the reflectivity and transmissivity related to the direct radiation, and $\bar{R}$ and $\bar{T}$ for

the diffuse radiation. The variable $\mu_0$ is the cosine zenith angle. As in the Briegleb [1992] parameterisation, the diffuse reflectivity was set to zero for the cases where $w$ is very small, because mathematically using this formulation, $\bar{R}$ can be less than zero.

#### 4.1.4.2 Layer Adding Method

The transmissivity and reflectivity computed for each layer in the previous section are now combined between two consecutives layers to determine the total transmission and reflection properties, taking into account the successive back and forward reflections. The equations for the total reflection and transmission to direct and diffuse radiation between two layers (Liou [1992] and Briegleb [1992]) are,

$$R_{12}(\mu_0) = R_1\mu_0 + \frac{\bar{T}_1((T_1(\mu 0) - e^{-\frac{\tau_1^\star}{\mu_0}})\bar{R}_2 + e^{-\frac{\tau_1^\star}{\mu_0}}R_2(\mu_0))}{1 - \bar{R}_1\bar{R}_2} \tag{4.9a}$$

$$T_{12}(\mu_0) = e^{-\frac{\tau_1^\star}{\mu_0}}T_2(\mu_0) + \frac{\bar{T}_2((T_1(\mu 0) - e^{-\frac{\tau_1^\star}{\mu_0}}) + e^{-\frac{\tau_1^\star}{\mu_0}}R_2(\mu_0)\bar{R}_1)}{1 - \bar{R}_1\bar{R}_2} \tag{4.9b}$$

$$\bar{R}_{12} = \bar{R}_1 + \frac{\bar{T}_1\bar{R}_2\bar{T}_1}{1 - \bar{R}_1\bar{R}_2} \tag{4.9c}$$

$$\bar{T}_{12} = \frac{\bar{T}_1\bar{T}_2}{1 - \bar{R}_1\bar{R}_2} \tag{4.9d}$$

Figure 4.5 shows a schematic plot of the combination between layer 1 and 2. This formulation is called the adding layer method and transforms homogeneous problems (the solution for one layer) to an inhomogeneous system.

For the computation of the spectral upward and downward fluxes at every layer interface we need to combine the layers over the entire column. The equations were obtained from the results of combining the layers using the above method upward in altitude, starting from the surface to the top, and in the downward direction:

$$F_{up} = \frac{e^{-\frac{\tau^\star}{\mu_0}}R_{up}(\mu_0) + (T_{dn}(\mu_0) - e^{-\frac{\tau^\star}{\mu_0}})\bar{R}_{up}}{1 - \bar{R}_{dn}\bar{R}_{up}} \tag{4.10a}$$

$$F_{dn} = e^{-\frac{\tau^\star}{\mu_0}} + \frac{(T_{dn}(\mu_0) - e^{-\frac{\tau^\star}{\mu_0}}) + e^{-\frac{\tau^\star}{\mu_0}}R_{up}(\mu_0)\bar{R}_{dn}}{1 - \bar{R}_{dn}\bar{R}_{up}}. \tag{4.10b}$$

In equations 4.10, $\tau^\star$ is the total optical depth above the interface, $\bar{R}_{up}/\bar{R}_{dn}$ is the reflectivity below/above the interface due to the diffuse radiation from above/below, $T_{dn}(\mu_0)$ is the total transmission to downward direct solar radiation and $R_{up}(\mu_0)$ is the reflectivity to upward direct solar radiation.

#### 4.1.4.3 K-Distribution Method

The K-Distribution Method (KDM) was developed to reduce the integration time of the transmission's calculation by line-by-line methods that are impracticable for general circulation model applications. The KDM keeps a good result accuracy and consists in applying to each predefined spectral band a reorganization in the ascending order of the absorption coefficients by their strength Lacis and Oinas [1991]. k($\lambda$) is mapped from spectral space to a space defined by the cumulative probability function g(k). The code integrates for each spectral fraction defined in the K-Tables the respective solar net flux for every model layers' interface and then multiplies by $\Delta$g. The net fluxes are then summed spectrally to compute the solar heating.

#### 4.1.4.4 Results

The spectral integrated and globally averaged absorbed solar flux obtained from the atmospheric condition used is 169.2 $W/m^2$. This result corresponds to a bolometric albedo of 0.756, and is close to the values observed. Figures 4.6(a) and 4.6(b) show the heating rates for two zenith angles and the spectral integrated downward and upward fluxes. The results are also compared with the work from Crisp [1986].

Below the clouds, in the lower atmosphere, we included an additional absorption within the spectral range 0.4 - 1.0 $\mu m$. The need of this correction was first noticed by Tomasko et al. [1980]. We think that this fault in our model is due to the absent representation of the hot-bands of $CO_2$ in this spectral region. The correction was done by adding an empirical blue gas absorber with an absorption coefficient increasing linearly with decreasing wavelength. It was also increased the effect of the Rayleigh scattering in this spectral region to have a good match with the integrated upward and downward fluxes from Crisp [1986] results, who calibrated his results with Pioneer Venus Sounder probe solar radiometer data.

Above the lower atmosphere the results are in good agreement with Crisp [1986] up to 93 km of altitude where the differences are less than $10\%$ (we use a similar cloud structure). An altitude of 93 km corresponds to the altitude just below the artificial sponge that avoids the reflection of any wave imposed by the rigid lid in the GCM (described in subsection 2.1.2). In the 3 highest layers, that are dominated by the absorption of $CO_2$, the results differences increase. For the gas absorption of $H_2O$ and $CO_2$, Crisp [1986] uses a more accurate method based on a line-by-line formalism.

The presence of the UV absorber in the clouds is well noticed in the heating rates profile: the bump with a maximum at 66 km, and the sudden drop in the downward solar flux. Interesting applications will be done in the Venus GCM, once the new solar radiation code allows changes in the distribution of the UV absorber during the integration of the model, which can affect the static stability of the atmosphere.

## 4.2 Thermal Radiation Scheme

Fast and accurate computations of the atmosphere's energy exchange via infrared radiation for long periods of integration, has been a challenging problem within the Venus GCM

community. Here we adapt the Net-Exchange parameterisation of thermal IR radiative transfer in Venus's atmosphere from Eymet et al. [2009] and Dufresne et al. [2005] and develop a new alternative formulation to compute the cooling rates.

The implementation of a physically-based IR radiative representation in a Venus GCM, has some extra difficulties due to its particular atmosphere, which is mainly composed of $CO_2$ with a huge optical thickness and clouds with high single-scattering albedo in some important spectral ranges. The two algorithms proposed in our research, are simple codes capable of rapidly computing the exchanges of IR radiative energy between different layers of the atmosphere, surface and space.

### 4.2.1 Net-Exchange Rate Matrix

The Net-Exchange Rate (NER) formalism adopted for the IR, is based on ideas originally proposed by Green [1967], and applied initially in a Venus GCM by Lebonnois et al. [2005]. Its result is a matrix that corresponds to a vertical discretisation of $n$ layers of the atmosphere plus the surface and the space. The definition of the NER in a given wavelength band ($\Psi$(i,j)) between two elements of the vertical discretisation (i and j) is the power emitted by j and absorbed by i, minus the inverse: the power emitted by i and absorbed by j. If $\Psi$(i,j) $>$ 0, this means that the element i absorbs more than emits in the exchanges with j. The matrix $\Psi$(i,j) has properties of an antisymmetric matrix, $\Psi$(i,j) = - $\Psi$(j,i), and since the exchanges of energy within i are not permitted, all the elements of the matrix diagonal are zero. The amplitude of each $\Psi$(i,j) depends mainly on three properties:

- the difference in temperature between i and j;
- the local emission and absorption of i and j;
- the attenuation of radiation along the optical path between i and j.

#### 4.2.1.1 Adaptation of the NER Formalism

The adaptation of the NER formalism to the GCM code has been done based on a simple parameterisation, Dufresne et al. [2005],

$$\Psi_{nb}(i,j) = \overline{\xi}_{nb}(i,j)(B_{nb}(j) - B_{nb}(i)). \tag{4.11}$$

The Net-Exchange Rates for each narrow wavelength band ($\Psi_{nb}$(i,j)) are evaluated from the difference in the Planck function at the mass weighted averaged temperatures for different layers, i and j, multiplied by an exchange factor $\overline{\xi}$(i,j) obtained with a complete radiative transfer model (KARINE) which depends on optical and physical properties of the atmosphere. Maintaining the atmospheric composition constant and assuming that variations in temperature do not affect the absorption and scattering cross sections, the values for $\overline{\xi}_{nb}(i,j)$ stay the same, which means that approximately $\Psi_{nb}(i,j)$ depends only on the temperature profile.

This simple parameterisation obeys the reciprocity and energy conservation principles. Any upgrade to this parameterisation, as to include some sensitivity to cloud variations in composition or in structure, cannot violate any of these principles. One possible extension is to include the sensitivity of the opacity to temperature variations which can be obtained from analytic results available in Eymet et al. [2009] for the upper atmosphere and, (in approximation), extended for all altitudes.

#### 4.2.1.2 KARINE

As noted above, the exchange factor $\overline{\xi}$(i,j) is computed using a complete radiative transfer model that assumes a reference atmosphere with composition and structure that is constant in time, due to the difficulties in computing efficiently $\overline{\xi}$(i,j) in a GCM. The radiative transfer model KARINE, which is based on a Net-Exchange Monte-Carlo algorithm (Eymet et al. [2009]), uses the gas and cloud spectra to produce $\overline{\xi}$(i,j) for 37 layers of the atmosphere (the future vertical discretisation that will be used in the Oxford Venus GCM) and a spectral range from 1.71 to 250$\mu$m.

The correlated-k coefficients for a particular atmospheric composition of $CO_2$, $H_2O$, $SO_2$, CO, HDO, $H_2S$, HCl and HF were computed in Eymet [2007]. Coupled with these data, the properties and distribution from an altitude of 47 to 80 km, of four different particle modes from a cloud model were included (Zasova et al. [2007]) and also the collision induced continuum absorption for $CO_2 - CO_2$ and $H_2O - H_2O$ (Moskalenko et al. [1979] and Gruszka and Borysow [1997]). From these data the KARINE code computed the net exchange factor $\overline{\xi}$(i,j) needed.

#### 4.2.1.3 Implicit Sheme

An implicit scheme was used to avoid numerical instabilities in the computation of the heating rates in the upper layers, where the total mass of each layer decreases rapidly with altitude. The method for the temporal integration of the temperature uses the following equation to define the net exchange rates of energy (Dufresne et al. [2005]),

$$\psi(i)^{\alpha} = \psi(i)^{t} + \alpha \sum_{j} \xi(i,j)^{t} \left(\frac{dB}{dT}|_{T_j}(T(j)^{t+\delta t} - T(j)^{t}) - \frac{dB}{dT}|_{T_i}(T(i)^{t+\delta t} - T(i)^{t})\right), \tag{4.12}$$

where the variable $\alpha$ can be equal to 1 (implicit formulation), 0.5 (semi-implicit formulation) and 0 (explicit formulation). In our code $\alpha$ is equal to 1 which is a formulation unconditionaly stable.

#### 4.2.1.4 IR Radiative Budget and Net-Exchange Rate matrix

Figure 4.7 shows the NER matrix and the net radiative budget computed and already adapted for the vertical resolution of the Venus GCM. The VIRA temperature profile was used.

The NER matrix and the net radiative budget, Figure 4.7, show some interesting features regarding the interaction radiation-atmosphere. In the deep atmosphere, the net exchanges between layers are more relevant with their close neighbours, due to the strong opacity from the overlapping of gaseous absorption lines caused by high pressures. At wavelengths for which the gas of the atmosphere is quite transparent but not for the continuum absorption by cloud droplets, a warm peak in the cloud bottom is produced, being visible in the net radiative budget and in the long wings of the NER matrix plot. The backscattering affects the NERs below and above the clouds. The cloud deck from 47 km to 57 km, heats from the lower part and cools from the upper part where in the inside of the cloud the radiative exchanges are quite complex due to the importance of scattering. Above the cloud, the atmosphere allows longer exchanges of energy than what is observed in the lower atmosphere due to the less intense effect of the pressure broadening. For these layers which are heated by the deep atmosphere, the exchanges with space are very important, resulting in its cooling. The space and the ground are continuous absorbers settled at a temperature of 3 K and 735 K respectively.

### 4.2.2 New Thermal Radiation Code

The NER matrix code from the previous subsection has important limitations such as the need of a new exchange matrix for variations in the atmospheric composition or variations in surface pressure. There are other technical problems related to the difficulties of handling the specific input for the KARINE software. As an alternative, we develop a thermal radiation code fast and accurate enough to be used for Venus Climate studies.

The method used is based on an absorptivity/emissivity formulation (neglects the scattering), that allows changes in the opacity structure and in the cloud structure with little computational time during the GCM integration. The code also permit a better control of consistency between the opacity used in the new solar radiation code and the one used here (the same gas and aerosol densities).

The results shown in Crisp and Titov [1997] suggest that the errors in the cooling rates are no larger than $10\%$ for almost all the atmosphere if we ignore the effects of the multiple scattering by the gases and aerosols at the thermal infrared wavelengths (Figure 4.8). The largest errors occur at the near-infrared wavelengths, where the clouds act almost as pure scatterers. A possible formulation for the thermal radiation that takes into account the scattering (more expensive in terms of computational time) would be using the same scheme from section 4.1.1($\delta$-Eddington-Adding code) and adding a thermal source function in each layer.

#### 4.2.2.1 Optical Properties of the Venus Atmosphere for Thermal Radiation

#### 4.2.2.2 Gases

In the spectral region studied in this part of the section ($1.7 - 50.1\mu m$) the main gaseous absorption lines in the Venus atmosphere are due to the molecular rotational transitions of $CO_2, H_2O$ and $SO_2$. The coefficients of absorption for these three gases were obtained using the K-Tables explained in the section regarding the solar radiation code.

To reduce the integration time to compute the cooling rates, we averaged the coefficient of absorption within a spectral band using the following equation,

$$k(\lambda, p, T, q_{H_2O}, q_{SO_2})) = \sum_i (k_{CO_2}(\lambda, p, T) + \frac{q_{H_2O}}{q_{CO_2}} k_{H_2O}(\lambda, p, T) + \frac{q_{SO_2}}{q_C O_2} k_{SO_2}(\lambda, p, T)) \Delta g_i \tag{4.13}$$

where $q_{H_2O}$ and $q_{SO_2}$ are the mixing ratios for $H_2O$ and $SO_2$, and $q_{CO_2}$ is the mixing ratio of $CO_2$ which is assumed to be well mixed in the atmosphere. $\Delta g_i$ are the spectral fractions within each spectral band defined in the K-Tables. In this formulation $k$ is considered as the coefficient of absorption of a single-mixture gas where the optical depth can be calculated using,

$$\tau(\lambda) = q_C O_2 \int k(\lambda, p, T) \rho_a dz. \tag{4.14}$$

$\rho_a$ is the air density.

#### 4.2.2.3 Aerosols

The cloud model adapted to test this new code is the same one used in the solar radiation section to keep the cloud structure consistent for future GCM applications. The optical properties used were interpolated from Crisp [1989] for $0.1\mu m$ spectral resolution between 1.7 and $50.1\mu m$.

#### 4.2.2.4 Continuum Absorption

The conditions that we find in the Venus atmosphere, high temperatures and pressures, produce an extra opacity due to the molecules' collisions. The phenomenon induces a continuum of absorption that in Venus is mostly due to $CO_2 - CO_2$ and $H_2O - H_2O$ collisions. The important contribution of the $CO_2$ molecules is not included in the actual code yet, which causes inaccurate results in the deep atmosphere. In the future, a parameterisation based on the experimental data from Moskalenko et al. [1979] will be implemented.

The continuum due to the $H_2O$ molecules implemented, is based on the sum of self-broadening and foreign broadening components. The empirical equation (McGouldrick [2007]) that defines the continuum absorption of the water vapor is given by,

$$k_{con,wv} = \sigma_s (X_{wv} P + \frac{\sigma_n}{\sigma_s}(1 - X_{wv}) P) \tag{4.15}$$

where $\sigma_s$ is the self-broadening and $\sigma_n$ is the foreign broadening component, and $X_{wv}$ is the number mixing ratio of the $H_2O$ molecule. $\sigma_s$ is defined as,

$$\sigma_s = e^{c(\frac{T_r}{T})-1}(a + be^{-\frac{b}{\lambda}}). \tag{4.16}$$

The empirical constants at a reference temperature ($T_r$) of 296 K (Roberts et al. [1976]) and the value of $\frac{\sigma_n}{\sigma_s}$ (Liou [1992]) are in the Table 4.3.

| Constant | $H_2O$ |
|---|---|
| a | 0.01 $\frac{cm^2}{gatm}$ |
| b | 120.0 $\frac{cm^2}{gatm}$ |
| c | 6.08 |
| $\beta$ | 0.002 |
| $\frac{\sigma_n}{\sigma_s}$ | 0.002 |

Table 4.3: Empirical constants for water vapor continuum from Roberts et al. [1976] and Liou [1992].

#### 4.2.2.5 Thermal Emission From an Isolated Layer

The differential emission equation used within a layer is defined such as,

$$dE(\mu) = B(\tau')e^{-\frac{\tau}{\mu}}\frac{d\tau'}{\mu} \tag{4.17}$$

where $\mu = cos(\theta)$ ($\theta$ is the emission angle), $\tau$ the optical depth ($\tau'$ is a point in the relative scale given by $\tau$ within the layer) and $B(\tau')$ is the spectrally integrated Planck function for one spectral band. $B(\tau')$ is defined as,

$$B(\tau') = B(T_t) + \frac{\tau'}{\tau}(B(T_b) - B(T_t)) \tag{4.18}$$

where $T_t$ is the temperature at the top edge of the layer and $T_b$ at the bottom edge. This formulation requires assuming that the temperature within the layer is linear in Planck function (Lacis and Oinas [1991]). Integrating equation 4.17 for the entire layer in a spectral interval, the intensity of the thermal radiation emitted in the upward direction is,

$$E(\mu) = B(T_t) - B(T_b) + (B(T_b) + \frac{\mu}{\tau}(B(T_b) - B(T_t)))(1 - e^{-\frac{\tau}{\mu}}). \tag{4.19}$$

The fraction $\frac{\mu}{\tau}$ causes problems in the computation of this equation for very small optical thickness. To avoid the singularity we use in the case of small $\tau$ the sum of terms of the series (we sum until n equals 7),

$$E(\mu) = \sum_{n=1}^{7}(-1)^{n+1}\frac{B(T_t) + nB(T_b)}{(n+1)!}(\frac{\tau}{\mu})^n \tag{4.20}$$

For the downward direction the equations are,

$$E^{\star}(\mu) = B(T_b) - B(T_t) + (B(T_t) - \frac{\mu}{\tau}(B(T_b) - B(T_t)))(1 - e^{-\frac{\tau}{\mu}}) \tag{4.21}$$

and

$$E^{\star}(\mu) = \sum_{n=1}^{7}(-1)^{n+1}\frac{B(T_b) - nB(T_t)}{(n+1)!}(\frac{\tau}{\mu})^n. \tag{4.22}$$

#### 4.2.2.6 Thermal Emission From Stacked Layer Atmosphere

The method used to combine the emission/absorption for all the physical homogeneous layers followed the vertical inhomogeneity atmosphere representation from Lacis and Oinas [1991]. Using the thermal emissions from isolated layers described above we use a simple formulation to obtain the outgoing upward thermal intensity (U) for each spectral band at the top of the nth layer,

$$U_0(\mu_i) = B(T_g r) \tag{4.23a}$$

$$U_1(\mu_i) = E_1(\mu_i) + U_0(\mu_i)e^{-\frac{tau_1}{\mu_i}} \tag{4.23b}$$

$$U_n(\mu_i) = E_n(\mu_i) + U_{n-1}(\mu_i)e^{-\frac{\tau_n}{\mu_i}} \tag{4.23c}$$

where $T_{gr}$ is the tempterature of the ground. $\mu_i$ represents the possible different directions and the indices on U, E and $\tau$ indicate the level number (0 is the surface and N the top layer of the stack).

The equations for the downward direction are,

$$D_N(\mu_i) = 0 \tag{4.24a}$$

$$D_{N-1}(\mu_i) = E_N^{\star}(\mu_i) + D_N(\mu_i)e^{-\frac{\tau_N}{\mu_i}} \tag{4.24b}$$

$$D_n(\mu_i) = E_{n+1}^{\star}(\mu_i) + D_{n+1}(\mu_i)e^{-\frac{\tau_{n+1}}{\mu_i}}. \tag{4.24c}$$

The downward intensity at the top of the model's atmosphere ($D_N(\mu_i)$) was assumed to be zero.

The upward and downward fluxes at each interface layer are simply calculated from the upward and downward intensities described above using the equations,

$$F_n^{\uparrow} = U_n(\bar{\mu})r \tag{4.25a}$$

$$F_n^{\downarrow} = D_n(\bar{\mu})r. \tag{4.25b}$$

On these equations we use a diffusivity factor $r$ to simplify the angular integration. This topic is described in the next part of the section.

From the above equations we can obtain the thermal cooling rates computing the divergence of the fluxes that are summed for all spectral bands and for each layer.

#### 4.2.2.7 Diffusivity Aproximation

The thermal intensities are evaluated for specific directions and the computation of the atmospheric cooling rates requires the integration over a hemisphere. The time spent by the radiation code integration can be largely affected by the choice of the method used for the integration over the emission angle. The method adopted in this work was the diffusivity approximation instead of other fast methods such as the Gaussian quadrature (Lacis and Oinas [1991]). The diffusivity approximation consists in the use of a diffusivity

factor r $\equiv \bar{\mu}^{-1}$, where $\bar{\mu}$ is the mean inclination and the best-fit function over the optical depth is (Ramanathan et al. [1985]),

$$r = 1.5 + \frac{0.5}{1 + 4\tau + 10\tau^2}, \tag{4.26}$$

#### 4.2.2.8 Radiative Fluxes and Cooling Rates

The new thermal radiation code which neglects the scattering takes 0.012 seconds to compute the spectral integrated fluxes and the cooling rates for a column of 37 layers. The time measurement is done after the calculation of all the optical properties present in the atmosphere.

The results shown in Figure 4.9(a) and 4.9(b) are preliminary. The code needs to be further tested with studies on the sensitivity to important physical properties and reviewed to fix some possible technical problems.

The heating rates and the fluxes obtained are very sensitive to the cloud distribution and temperature of each layer. In this work we used similar cloud distribution from 4.1.4 and a temperature profile close to the one used in Crisp [1989].

The induced continuum absorption phenomenon due to the collision of $CO_2$ molecules gives an important contribution to the cooling rates in the deep atmosphere, which is not taken into account yet in this code. This problem makes the comparison studies with other models for the deep atmosphere difficult. However for the mesosphere this effect is less important and we compare the heating rates obtained with our code with those obtained by Crisp [1989] (Figure 4.9(b)). In general our heating rates are in good agreement, despite the problems in the upper atmosphere and our lower vertical resolution.

## 4.3 1D Radiative-Convective Model

The radiative equilibrium temperatures were found using a 1D radiative-convective model that also includes a soil temperature parametrisation. The initial vertical temperature structure was very close to the VIRA model. The time step used was 2 hr, which is smaller than the radiative relaxation time in the Venus mesosphere and guarantees the stability of the model. The thermal equilibrium was reached when the temperature variation in each model's layer, $T_t$-$T_{t-\delta t}$, was less than 0.02$^o$ K.

The heating profiles used were obtained using a global-averaged solar heating rates of the new solar radiative code,

$$\frac{dT}{dt}(p) = \frac{1}{2}\int_0^{\frac{\pi}{2}} \frac{dT}{dt}(\theta_z, p) sin(\theta_z) d\theta_z, \tag{4.27}$$

where $\theta_z$ is the zenith angle. The integral was evaluated using a Gauss-Legendre quadrature method, 8 point rule.

The Net-Exchange Rate (NER) Matrix code was used to simulate the cooling in the atmosphere via thermal radiation.

### 4.3.1 Soil Model

The 1D model includes a simplified parameterisation to simulate the evolution of the temperatures in the subsurface. The temperature surface is also affected by this formulation due to the interchanges of thermal conduction in the soil. The parameterisation was developed for the UK-French Mars GCM (Hourdin et al. [1993]).

The conduction equation that is used to update the temperatures is,

$$\frac{\partial T}{\partial t} = \frac{1}{C}\frac{\partial}{\partial z}(-\lambda\frac{\partial T}{\partial z}) \tag{4.28}$$

where $C$ is the specific heat per unit volume and $\lambda$ is the soil conductivity. The soil thermal inertia (I = $\sqrt{\lambda C}$) used is equal to 2200 $Jm^{-2}K^{-1}s^{-\frac{1}{2}}$ (C. Wilson, private communication, 2010).

The parameterisation uses also a multilayer soil formulation (10 layers) that was developed by Warrilow et al. [1986], which produces accurate results for responses to variations of the temperature forcing at the surface.

### 4.3.2 Method of Convective Adjustment

The convective adjustment method consists in adjusting the lapse rate to the critical lapse rate whenever the lapse rate is exceeded during the model's integration (Manabe and Strickler [1964]).

The first model layer (shallow layer near the surface) is assumed to be a non-convective layer to avoid instability problems due to the NER code's sensitivity to fast variations of the temperature near the surface. The convective layers should obey the equation,

$$\frac{C_p}{g}\int_{P_t}^{P_b}(\frac{\partial T}{\partial t})^{\tau}_{NET}dp = \frac{C_p}{g}\int_{P_t}^{P_b}(\frac{\partial T}{\partial t})^{\tau}_{RAD}dp, \tag{4.29}$$

when the stability criterion is not satisfied (lapse rate smaller than the critical lapse rate). $P_b$ and $P_t$ are the pressure at the bottom and top of each layer. The variables $C_p$ and g, are the specific heat of air at constant pressure and the acceleration of gravity. A repeatedly upward iteration (from the second layer to the top) is used until the layers of supercritical lapse rate are completely removed.

### 4.3.3 Thermal Equilibrium

An atmosphere in thermal equilibrium does not have rapid changes of temperature in each layer. This state is characterized by: the condition of local radiative equilibrium in each layer, the net incoming solar radiation and the net outgoing thermal radiation are the same at the top of the model's atmosphere, and the excess of solar radiation absorbed at the surface is compensated by an equal amount of energy emitted as thermal radiation.

Table 4.4 and Figure 4.10 show the results obtained by this model after 88 Earth days of integration. The number of layers used in this chapter is 37, where we included 3 extra

layers in the deepest atmosphere to better suit the future boundary layer turbulence and topographic surface parameterisation (chapter 6).

The absolute lapse rate near 60 km (in the mesosphere) is higher than would be expected, comparing with the VIRA temperature profile. The cause of this phenomenon is related with the cooling to space that should be stronger in this region. One possible solution for this problem would be to calibrate the number density of the aerosols which does not seem the most appropriate. The temperatures for the lower atmosphere are very close to the values from the VIRA temperature profile. The 1D model reached the thermal equilibrium too fast for significant temperature variations in this region be observed. The use of a smaller value for $T_t$-$T_{t-\delta t}$ is required but just after the correction of the cloud distribution mentioned above. A wrong cloud distribution can induce wrong temperatures in the lower atmosphere.

In general, after a calibration of the input in the KARINE program to fix the cloud distribution profile, the new radiative scheme is capable of rapidly and accurately computing the energy exchange in the atmosphere. This simple parameterisation based on radiative transfer formulation, gives a more realistic picture of the energy exchange in the atmosphere than the Newtonian cooling approach.

| # level | T $[K]$(VIRA) | Pressure $[mbar]$ | T $[K]$ | SW Q$[K\ day^{-1}]$ | LW Q$[K\ day^{-1}]$ |
|---|---|---|---|---|---|
| 1 | 732.6 | 92000.00 | 733.3062 | 4.4085E-04 | -3.7966E-03 |
| 2 | 732.2 | 91723.95 | 732.8197 | 4.4606E-04 | -3.7331E-03 |
| 3 | 731.4 | 91125.76 | 731.9560 | 4.6020E-04 | -3.6230E-03 |
| 4 | 729.2 | 89511.15 | 729.8771 | 5.0665E-04 | -3.0705E-03 |
| 5 | 721.2 | 84032.41 | 722.4528 | 6.1734E-04 | -1.7404E-03 |
| 6 | 706.6 | 74687.24 | 708.5845 | 8.2150E-04 | -1.5913E-03 |
| 7 | 688.4 | 64274.07 | 691.1348 | 1.1283E-03 | -2.0784E-03 |
| 8 | 667.4 | 53780.45 | 670.8367 | 1.5514E-03 | -1.4931E-03 |
| 9 | 644.4 | 43898.96 | 648.6448 | 2.1134E-03 | -2.0047E-03 |
| 10 | 621.7 | 35042.68 | 625.2094 | 2.8332E-03 | -4.5006E-03 |
| 11 | 598.7 | 27401.29 | 599.4863 | 3.7154E-03 | -5.06036E-03 |
| 12 | 572.0 | 21003.60 | 572.0573 | 4.7436E-03 | -5.7270E-03 |
| 13 | 543.1 | 15786.69 | 543.6238 | 5.9044E-03 | -4.9868E-03 |
| 14 | 514.1 | 11637.86 | 514.4113 | 7.2405E-03 | -4.3094E-03 |
| 15 | 484.1 | 8407.997 | 484.6818 | 8.8095E-03 | -7.1958E-04 |
| 16 | 454.9 | 5945.858 | 456.1151 | 1.0613E-02 | 1.7684E-03 |
| 17 | 427.6 | 4109.509 | 429.2419 | 1.2735E-02 | -2.0792E-04 |
| 18 | 403.6 | 2770.290 | 404.0859 | 1.5384E-02 | -2.0397E-02 |
| 19 | 381.7 | 1817.145 | 376.4434 | 1.8390E-02 | 0.1596 |
| 20 | 356.0 | 1156.706 | 341.6081 | 4.6265E-02 | 0.3237 |
| 21 | 323.9 | 712.6051 | 306.0171 | 0.1192 | -0.6482 |
| 22 | 288.7 | 423.7187 | 270.2982 | 0.3265 | -1.5179 |
| 23 | 264.5 | 242.6378 | 251.0534 | 0.7971 | -0.8466 |
| 24 | 247.8 | 133.6820 | 253.5473 | 3.2859 | -3.3183 |
| 25 | 237.2 | 70.84885 | 252.6412 | 3.8113 | -3.8370 |
| 26 | 233.2 | 36.16577 | 241.0751 | 3.4605 | -3.4864 |
| 27 | 224.2 | 17.92996 | 233.1176 | 4.3639 | -4.3883 |
| 28 | 213.9 | 8.684272 | 226.5163 | 5.9359 | -5.9581 |
| 29 | 201.1 | 4.163791 | 219.1795 | 7.7336 | -7.7537 |
| 30 | 186.6 | 2.039423 | 210.3660 | 10.1758 | -10.1943 |
| 31 | 175.7 | 1.034929 | 203.1305 | 13.3210 | -13.3378 |
| 32 | 169.8 | 0.5604298 | 195.9909 | 17.9520 | -17.9669 |
| 33 | 166.3 | 0.3383125 | 188.0038 | 23.5023 | -23.5149 |
| 34 | 164.2 | 0.2340235 | 182.7126 | 22.7889 | -22.7997 |
| 35 | 162.6 | 0.1477210 | 171.1043 | 27.2143 | -27.2235 |
| 36 | 162.2 | 6.7841887E-02 | 160.0330 | 31.9537 | -31.9612 |
| 37 | 163.6 | 2.4472000E-02 | 139.3282 | 99.4174 | -99.4218 |

Table 4.4: Results of the radiative-convective equilibrium.

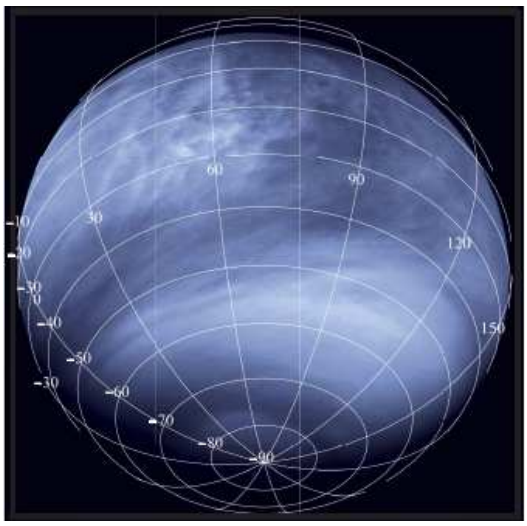


Figure 4.2: False-colour image from Titov et al. [2008] of the Venus' atmosphere using an ultraviolet filter, showing the remarkable dark features due to an unknown ultraviolet absorber.

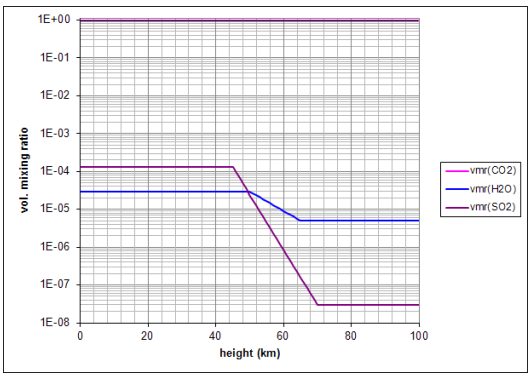


Figure 4.3: Volume mixing ratios of $CO_2$, $H_2O$ and $SO_2$.The values were obtained from VIRA model.

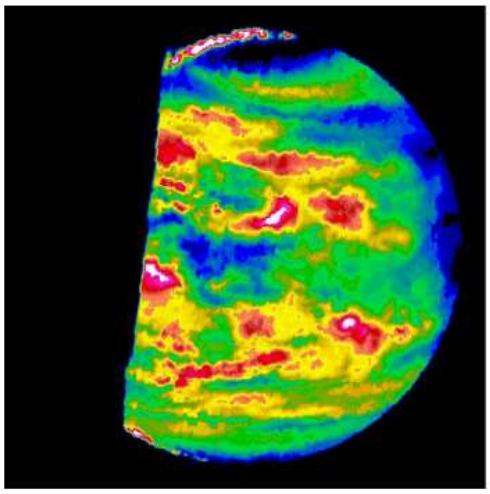

Figure 4.4: This false colour image is from the night side of Venus in the near-infrared 'window' at 2.3 $\mu$m, and was obtained by the NIMS aboard the Galileo spacecraft during its flyby in February 1990 [Carlson et al., 1991]. The variations (more than one order of magnitude) in brightness show the change in thickness of the clouds from white and red (thin cloud regions) to black and blue (thick clouds).

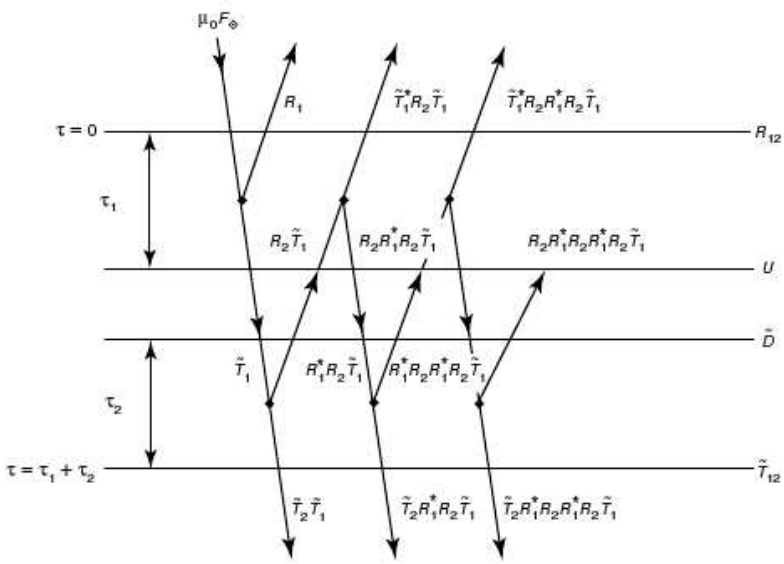


Figure 4.5: Illustration of the adding method configuration from Liou [2002].

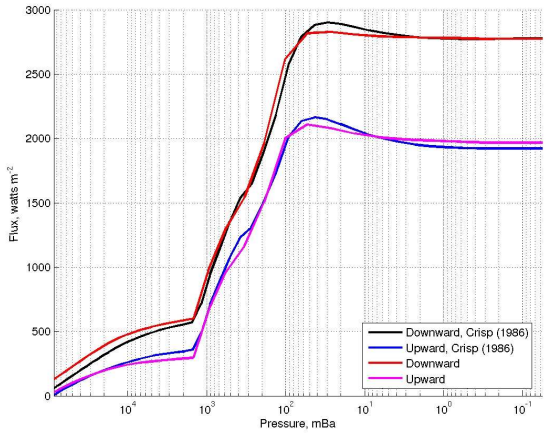


(a) Upward and Downward Fluxes.

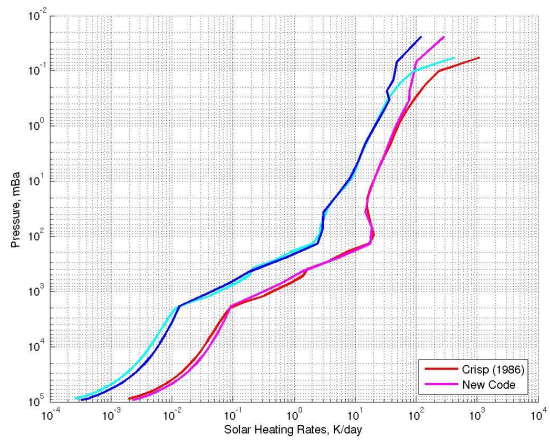


(b) Heating rates.

Figure 4.6: Compares the heating rates and the spectral integrated downward and upward fluxes of the new solar radiation code with the results from Crisp [1986]. The results shown are for two different zenith angles ($0^o$ and $75^o$).

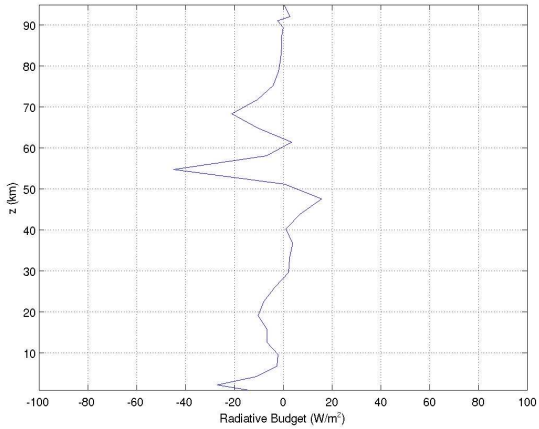


(a) Radiative Budget (W/m$^2$)

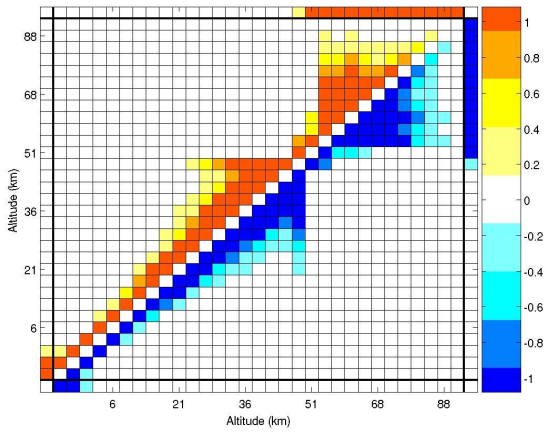


(b) Net Exchange Rate matrix (W/m$^2$)

Figure 4.7: **(a)** The radiative budget(W/m$^2$) as function of altitude. **(b)** The spectrally integrated Net Exchange Rate matrix.
Note: There are 37 atmospheric layers plus the space (layer index 39) and the surface (layer index 1). These last two act as black bodies.

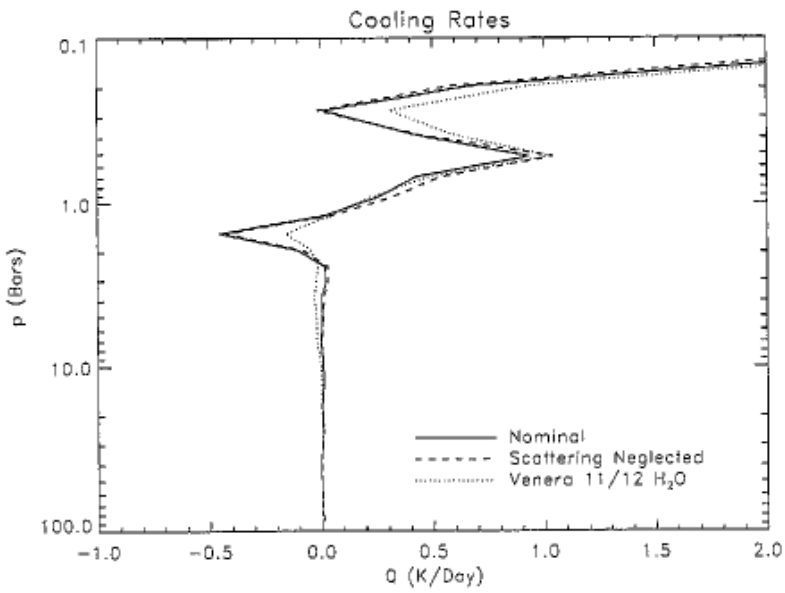


Figure 4.8: Effects of neglecting the multiple scattering in the Venus atmosphere at the thermal infrared wavelengths from Crisp and Titov [1997].

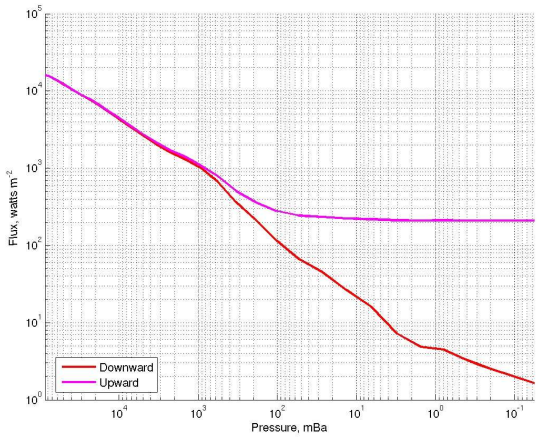


(a) Upward and Downward Fluxes.

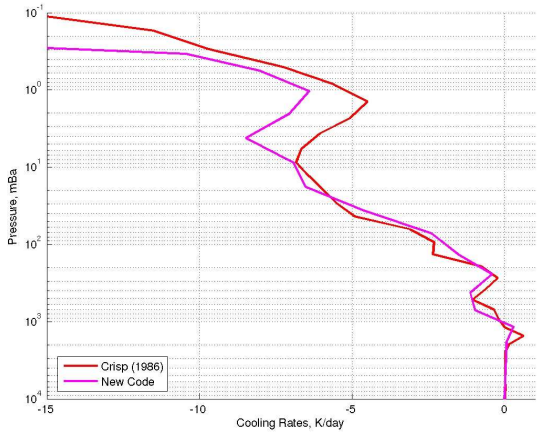


(b) Cooling rates.

Figure 4.9: The cooling rates and the spectral integrated downward and upward fluxes of the new thermal radiation code. Figure (**b**), compares the cooling rates with the results obtained by Crisp [1989].

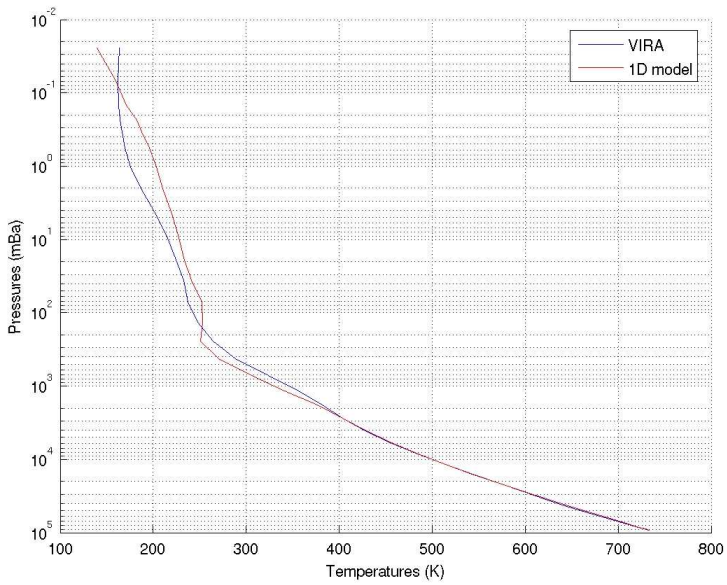


Figure 4.10: Comparison between the VIRA temperature profile and the results obtained in the global-mean radiative-convective 1D model.

CHAPTER 5

# Conclusions

The upward-integration of the thermal wind equation using the temperature maps obtained in the Venus SGCM, showed that the choice of the lower boundary condition and the presence of non-negligible eddy terms, are the main sources of errors in retrieving the zonal winds. The new method suggested in the previous section (Zonal winds on Venus) to better estimate the lower boundary, estimates an increase of the zonal winds mainly in the polar region. This increase is also present in the zonal thermal winds results (Figure 3.10) using observational temperature maps (VIRTIS data, Grassi et al. [2010]). The improved new results need to be validated with more observational data and with other methods that retrieve the zonal winds in the polar region. One method that could be used for comparison studies would be based on a similar formulation to the one used by Limaye [1985] with new data from the Venus Express Radio Science Experiment.

The Titan SGCM is in an early stage, and needs to be calibrated (mainly the parameters from the temperature forcing scheme) and compared with others models' results and with observations from probe missions. The first results showed in this report exhibit the influence of the seasons in the Titan' atmospheric circulation, which causes variations in the transport of angular momentum in the stratosphere. The results are preliminary and need to be explored before the important comparison studies with the Venus' atmospheric circulation.

The new solar radiative scheme tested to implement in the Oxford Venus GCM is capable of rapidly and accurately computing the heating rates in the atmosphere. This new code allows the GCM to have a self-consistent solar radiation formulation that will be used for the first time within the International Venus Climate Modelling Community. This scheme is now being introduced in the 3D numerical model. A particular advantage of the new solar radiation code is that it can take into account time-varying changes in the distribution of the UV absorber in the clouds (also computed dynamically in our model) during the model simulation.

For the thermal radiation two options are available: the Net-Exchange Rate (NER) formulation or the new thermal radiation code. These two codes can be used with the solar radiation code to build the new radiative transfer scheme of the Venus GCM. The new thermal radiation code has several advantages in relation to the NER formulation that was described in the section 4.2.2. For example, it is straightforward to maintain the same atmospheric composition as in the solar radiation code. The preliminary studies of this new code showed a fast scheme capable of accurately computing the cooling rates for different atmospheric conditions. In general, its versatility turns it into an interesting tool to be explored in the future.

From the results of the 1D radiative-convective model, we observed that in the mesosphere the temperature is warmer than expected. This problem is related to the cooling to space energy which is not enough from the NER calculation. To correct this problem the input in the KARINE code that builds the Net-Exchange Matrixes needs to be calibrated (especially the cloud distribution).

The promising results obtained for the new radiative codes are a motivation for the next step in this work, which will be to test this scheme in the Venus GCM.

CHAPTER 6

# Future Work

## Contents



My future plan of work will be to apply the tools developed in the last two years, to build the first Venus GCM that uses a complete and complex radiation scheme for solar and thermal spectra interacting with time-variable cloud cover. The new model will have the most realistic representation of the thermal tide and the cloud feedback in the atmospheric circulation. These features can help us to understand the global circulation and better interpret data from previous and current space missions (eg. Venus Express).

There are several theoretical dynamical mechanisms that can explain the formation of the super rotation on the Venus' atmosphere as mentioned in the introduction. However, it is unclear if one dominates in the Venus atmosphere, if it is more than one, or an undiscovered new mechanism. Our new model will help us to study in detail these mechanisms, verifying their validity, and thereby having a better understanding in what drives a slowly rotating planet like Venus to have a super rotating atmosphere. It will also be possible to study factors that determine the cloud distribution across the planet using our new model. This last feature in our GCM is totally new within the Venus GCM climate community.

The work from Lebonnois et al. [2010b] is the most complete Venus GCM to date and the only one published in the peer reviewed literature so far that has implemented with success a consistent radiative transfer calculation. However, their radiative parameterisation has significant limitations, such as the need to recompute the new exchange matrix for variations in the atmospheric composition or variations in surface pressures. They also maintain the cloud structure constant with latitude in the model, via the use of a precomputed table of solar fluxes from Crisp [1986] to calculate the solar heating rates. It is also important to point out that the solar and thermal radiation sections were not treated consistently in Lebonnois et al. [2010b], due to the two distinct cloud models assumed.

A Japanese group is also trying to implement a radiation scheme based on radiative transfer (Ikeda et al. 2008; Yamamoto et al. 2010). Their radiative transfer code is based on a parameterisation developed by Nakajima et al. [2000]. The code combines a k-distribution method with a discrete ordinate method for just 18 bands from the shortwave to the longwave. This work has not been published yet in the open literature, and the only known details are from conference proceedings. The details available are not enough for a rigorous appreciation of their work. From the little information available, it appears that the division of the spectrum seems too simplified to reproduce the effects of the complex

absorption/scattering adequately especially in the near infrared where the clouds play an important role. However, their GCM seems to produce results that are very similar to the one produced by Lebonnois et al. 2010b (with super rotation in the mesosphere but not in the lower atmosphere).

In my project so far, we have developed a radiation scheme which avoids at least some of the problems mentioned above. Our codes allow to recompute the optical properties of the atmosphere for the solar and thermal wavelength spectra in a computationally fast way during the GCM integration. The unrealistic weak winds in the lower atmosphere could be related to a poor representation of the radiative absorption in this region in previous work, and this subject will be explored in our future work.

The new radiation codes show promising results when compared with Crisp [1986] and Crisp [1989], who used more accurate models based on a line-by-line formulation to simulate the gases' absorption. The quantities compared were the heating/cooling rates and the radiative fluxes for a 1D atmospheric condition (for which the gases' concentrations were taken from the VIRA model and the cloud distribution from Crisp 1986). The next step will be to do a sensitivity study of the model's results when varying relevant physical quantities for several realistic atmospheric profiles (such as variations in temperature and cloud distribution) and improve the code structure for a faster integration to better suit GCM applications. The sensitivity studies will be validated with a more complex code (RADTRANS, Irwin et al. 2008).

It is important to define a global cloud structure and aerosols in the GCM. These two components of the atmosphere are crucial to define and quantify the deposition of the radiative energy in different regions of the atmosphere. Our plans are to first build an updated global zonally averaged cloud structure in collaboration with Joanne Barstow, which will be used simultaneously in our solar and thermal radiation codes. In an initial phase, this new global cloud structure will be static during the GCM integration though more realistic than the latitudinally uniform one assumed in Lebonnois et al. [2010b].

The Venus GCM running with the new cloud structure will provide the first important results. In a second step we will use the new radiation codes in conjunction with the cloud transport model implemented by Lee [2006]. These features allow the time variability in the cloud to interact with the radiative budget calculation. This innovative characteristic will distinguish our model from any other work, and will help us to have a better understanding of the cloud distribution in the atmosphere and its feedback on the circulation.

The first tests on the Venus GCM with the new radiative formulation are currently at an early stage, with the model starting from an atmosphere already in super rotation (a standard final result which was from the SGCM) and having just integrated for hundreds of Earth years. The run is still far from the expected "steady state" equilibrated regime. However it is already possible to see strong jets of around 75 $ms^{-1}$ at the predicted altitude (around 50 hPa) from observations.

Other parameterisation schemes in my work will also be included in our Venus GCM with lower priority: namely boundary layer turbulence and surface topography. These schemes will be adapted from the Unified Model. The boundary layer scheme will be based on a bulk transport turbulent mixing scheme (Jacobson 2005). Similar topography and boundary layer schemes have already been explored by Lee [2006], and our plans are to

implement them again, into further small improvements. The aim of the implementation of these two parameterisations is to have a better understanding of the role of the topography in the fully developed super rotation.

The final complete version of the Venus GCM will be studied by doing diagnostic computations of eddy statistics and other aspects of model climatology.

On the observational side, it is important to validate and verify the simulation using data from the Venera, Pioneer Venus missions and Venus Express. This work will be done by comparing the results of a reference Venus GCM simulation with previous observational studies, such as, for example, vertical profiles of the zonal winds (Schubert 1983), thermal structure of the atmosphere, solar thermal tides (Zasova et al. 2007; Grassi et al. 2010), atmospheric waves (Del Genio and Rossow 1990) and cloud distributions.

In the first year of my DPhil, we studied the possible existence of an atmospheric transport barrier at high latitudes from the results of the SGCM. Our plans, if we still have time, are to compute the effective diffusivity of a cloud tracer, and analyse potential vorticity (PV) in isentropic maps, exploring possible regions for this phenomenon. This is an important study also to understand the cloud distribution in the polar region of the Venus atmosphere (Titov et al. 2008 and Teanby et al. 2008).

In Lebonnois et al. [2010a] the results of different simplified GCMs have been compared. Using similar physical schemes and parameters the models produced different circulations. This raises the importance of the dynamical core in the atmospheric motion modelled. Our GCM uses a particular dynamical core called HadAM3, which means that even if we use similar physical parameterisations like the radiation scheme of other groups, the result obtained could be reasonably different and relevant to be studied.

Our model is an important step in the development of a complex model capable of reproducing the Venus climate. The radiation-cloud variability interaction parameterisation will be new and important for the study of the atmospheric circulation, cloud distribution and their influence in the dynamics of the atmosphere.

## 6.1 Further Activities

I had the opportunity to attend and present oral/poster presentations such as:

- J. Mendonca, P. L. Read, C. Wilson and S. R. Lewis, "New Radiative Transfer Code in the Oxford Venus GCM", Poster and 5 minutes oral presentation, International Venus Conference (Aussois, 2010).

- J. Mendonca, P. L. Read, and S. R. Lewis, "New results from the Oxford Venus GCM", Poster and 5 minutes oral presentation, International School in Planetary Atmospheres (Kobe - Center for Planetary Science, 2010). $https://www.cps-jp.org/pschool/2010-01-04/10\_poster/pub/P16\_Mendonca\_Joao\_poster.pdf$

- J. Mendonca, "Dynamics and circulation of Venus and Titan", Atmospheric, Oceanic and Planetary Physics Annual Retreat, 15 minutes oral presentation, Oxford, September 2009.

- J. Mendonca, P. L. Read, and S. R. Lewis, "Studies of Venus using a General Circulation Model", Atmospheric, Oceanic and Planetary Physics Seminars, 25 minutes oral presentation, Oxford, May 2010.

These meetings gave me a broad perspective of the work that has been done in planetary sciences, and the chance to meet and discuss with people who are working in my research area.

The one per term oral presentations in my research group's meeting (Geophysical and Planetary Fluid Dynamics group), were important in the way that I could improve presentation skills.

## 6.2 Approximate Timeline

It is always difficult to timeline the work that depends on the development of a numerical model, however, a suggested plan of work for the next two years is in Table 6.1.

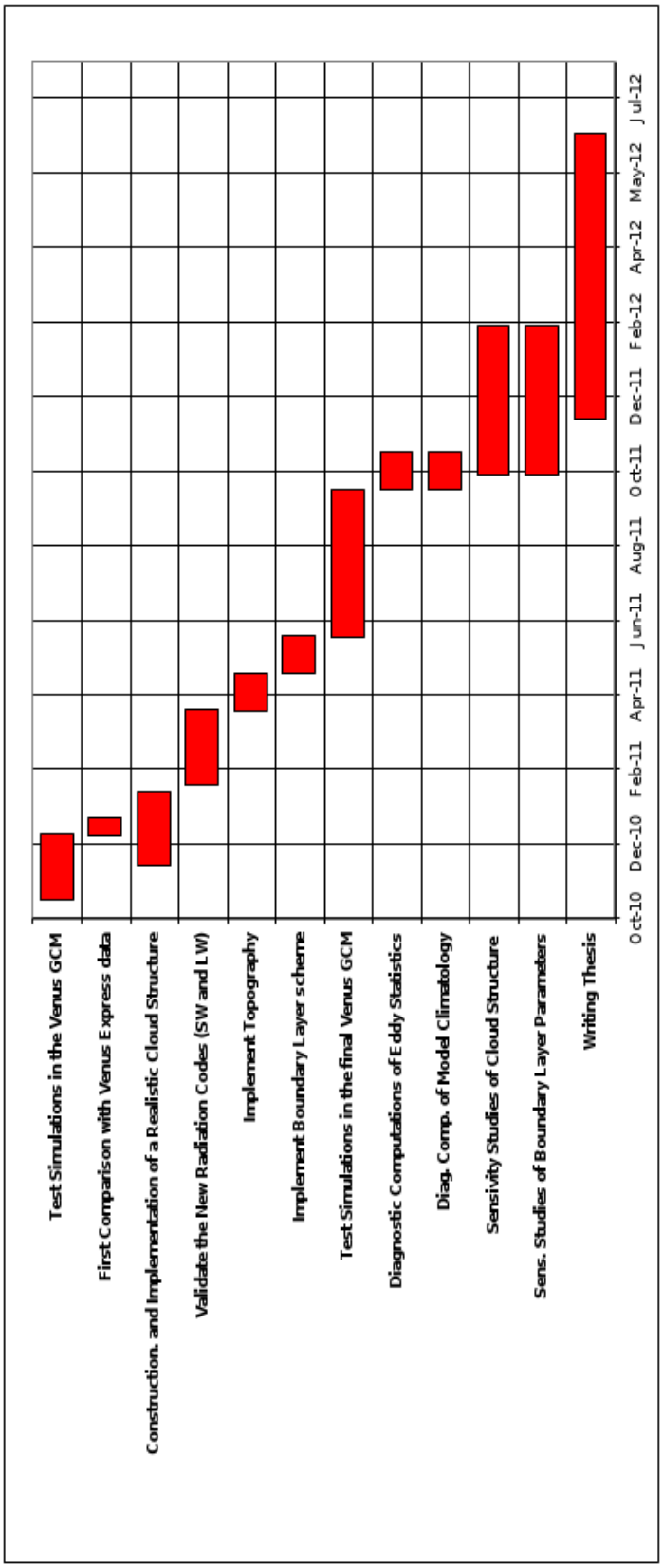


Figure 6.1: Future work timeline

## Acknowledgements

I thank my supervisors for the motivating ideas, suggestions and guidance. I acknowledge financial support from FCT - Fundação para a Ciência e a Tecnologia (Portugal).

# Bibliography


M. Allison and L. D. Travis. The Jovian Atmospheres. *NASA Conference Publication 2441, New York*, 1985. 13

D. G. Andrews, J. R. Holton, and C. B. Leovy. *Middle atmosphere dynamics.* 1987. 22, 24

A. Arakawa and V. R. Lamb. A potential enstrophy and energy conserving scheme for the shallow water equations. *Monthly Weather Review*, 109:18–36, 1981. doi: 10.1175/1520-0493(1981)109. 7

S. W. Bougher, M. J. Alexander, and H. G. Mayr. Upper Atmosphere Dynamics: Global Circulation and Gravity Waves. In S. W. Bougher, D. M. Hunten, and R. J. Philips, editors, *Venus II: Geology, Geophysics, Atmosphere, and Solar Wind Environment*, pages 259–+, 1997. 3

B. P. Briegleb. Delta-Eddington approximation for solar radiation in the NCAR community climate model. *J. Geophys. Res.*, 97:7603–7612, May 1992. 35, 36, 37

R. W. Carlson, K. H. Baines, L. W. Kamp, P. R. Weissman, W. D. Smythe, A. C. Ocampo, T. V. Johnson, D. L. Matson, J. B. Pollack, and D. Grinspoon. Galileo infrared imaging spectroscopy measurements at Venus. *Science*, 253:1541–1548, September 1991. doi: 10.1126/science.253.5027.1541. 50

J. A. Coakley, Jr., R. D. Cess, and F. B. Yurevich. The Effect of Tropospheric Aerosols on the Earth's Radiation Budget: A Parameterization for Climate Models. *Journal of Atmospheric Sciences*, 40:116–138, January 1983. doi: 10.1175/1520-0469(1983)040. 36

L. Colin. *Basic facts about Venus*, pages 10–26. 1983. 7

A. Coustenis and F. Taylor. *Titan : the earth-like moon*. 1999. 13

D. Crisp. Radiative forcing of the Venus mesosphere. I - Solar fluxes and heating rates. *Icarus*, 67:484–514, September 1986. doi: 10.1016/0019-1035(86)90126-0. 2, 32, 33, 34, 35, 38, 51, 59, 60

D. Crisp. Radiative forcing of the Venus mesosphere. II - Thermal fluxes, cooling rates, and radiative equilibrium temperatures. *Icarus*, 77:391–413, February 1989. doi: 10.1016/0019-1035(89)90096-1. 42, 45, 54, 60

D. Crisp and D. Titov. The Thermal Balance of the Venus Atmosphere. In S. W. Bougher, D. M. Hunten, & R. J. Phillips, editor, *Venus II: Geology, Geophysics, Atmosphere, and Solar Wind Environment*, pages 353–+, 1997. 41, 53

M. J. P. Cullen, T. Davies, and M. H. Mawson. Conservative finite diferences schemes for a unified forecast/climate model. . *Unified Model Documentation Paper No. 10. Meteorological Office, UK.*, 1992. 7, 12

A. D. Del Genio and W. B. Rossow. Planetary-scale waves and the cyclic nature of cloud top dynamics on Venus. *Journal of Atmospheric Sciences*, 47:293–318, February 1990. doi: 10.1175/1520-0469(1990)047. 4, 61

J.-L. Dufresne, R. Fournier, C. Hourdin, and F. Hourdin. Net Exchange Reformulation of Radiative Transfer in the $CO_2$ 15-$\mu$m Band on Mars. *Journal of Atmospheric Sciences*, 62:3303–3319, September 2005. doi: 10.1175/JAS3537.1. 39, 40

V. Eymet. KARINE: a tool for infrared radiative transfer analysis in planetary atmospheres. *Note internr, Laboratire d'Energétique, France*, 2007. 40

V. Eymet, R. Fournier, J.-L. Dufresne, S. Lebonnois, F. Hourdin, and M. A. Bullock. Net exchange parameterization of thermal infrared radiative transfer in Venus' atmosphere. *Journal of Geophysical Research (Planets)*, 114:11008–+, November 2009. doi: 10.1029/2008JE003276. 2, 39, 40

S. B. Fels and R. S. Lindzen. The Interaction of Thermally Excited Gravity Waves with Mean Flows. *Geophysical and Astrophysical Fluid Dynamics*, 6:149–191, 1974. doi: 10.1080/03091927409365793. 3

P. J. Gierasch. Meridional circulation and the maintenance of the Venus atmospheric rotation. *Journal of Atmospheric Sciences*, 32:1038–1044, June 1975. doi: 10.1175/1520-0469(1975)032. 3

D. Grassi, A. Migliorini, L. Montabone, S. Lebonnois, A. Cardesìn-Moinelo, G. Piccioni, P. Drossart, and L. Zasova. Thermal structure of Venusian nighttime mesosphere as observed by VIRTIS-Venus Express. *J. Geophys. Res.*, page in press., 2010. doi: 10.1029/2009JE003553. 20, 27, 28, 30, 57, 61

J. S. A. Green. Division of radiative streams into internal transfer and cooling to space. *Quarterly Journal of the Royal Meteorological Society*, 93:371–372, July 1967. doi: 10.1002/qj.49709339710. 39

M. Gruszka and A. Borysow. Roto-Translational Collision-Induced Absorption of CO_2 for the Atmosphere of Venus at Frequencies from 0 to 250 cmˆ-1, at Temperatures from 200 to 800 K. *icarus*, 129:172–177, September 1997. doi: 10.1006/icar.1997.5773. 40

J. E. Hansen and L. D. Travis. Light scattering in planetary atmospheres. *Space Science Reviews*, 16:527–610, October 1974. doi: 10.1007/BF00168069. 34

F. Hourdin, P. Le van, F. Forget, and O. Talagrand. Meteorological Variability and the Annual Surface Pressure Cycle on Mars. *Journal of Atmospheric Sciences*, 50:3625–3640, November 1993. doi: 10.1175/1520-0469(1993)050. 46

F. Hourdin, O. Talagrand, R. Sadourny, R. Courtin, D. Gautier, and C. P. McKay. Numerical simulation of the general circulation of the atmosphere of Titan. *Icarus*, 117: 358–374, October 1995. doi: 10.1006/icar.1995.1162. 11, 17

K. Ikeda, M. Yamamoto, and M Takahashi. Venus' superrotation simulated by an atmospheric general circulation model. pages Vol.3, EPSC2008–A–00419. European Planetary Science Congress, 2008. 59

P. G. J. Irwin, N. A. Teanby, R. de Kok, L. N. Fletcher, C. J. A. Howett, C. C. C. Tsang, C. F. Wilson, S. B. Calcutt, C. A. Nixon, and P. D. Parrish. The NEMESIS planetary atmosphere radiative transfer and retrieval tool. *Journal of Quantitative Spectroscopy and Radiative Transfer*, 109:1136–1150, April 2008. doi: 10.1016/j.jqsrt.2007.11.006. 60

M. Z Jacobson. *Fundamentals of Atmospheric Modelling*. 2005. 60

A. A. Lacis and V. Oinas. A description of the correlated-k distribution method for modelling nongray gaseous absorption, thermal emission, and multiple scattering in vertically inhomogeneous atmospheres. *J. Geophys. Res.*, 96:9027–9064, May 1991. doi: 10.1029/90JD01945. 32, 38, 43, 44

S. Lebonnois, F. Hourdin, V. Eymet, R. Fournier, and J.-L. Dufresne. A new Venus General Circulation Model, in the context of the Venus-Express mission. In *Bulletin of the American Astronomical Society*, volume 37 of *Bulletin of the American Astronomical Society*, pages 742–+, August 2005. 39

S. Lebonnois, C. Covey, C. Lee, S. R. Lewis, H. Parish, P. L. Read, G. Schubert, and M. Yamamoto. A comparative analysis of Simplified General Circulation Models of Venus atmosphere. *EGU General Assembly 2010, held 2-7 May, 2010 in Vienna, Austria, p.4953*, 12:4953–+, May 2010a. 61

S. Lebonnois, F. Hourdin, V. Eymet, A. Crespin, R. Fournier, and F. Forget. Superrotation of Venus' atmosphere analyzed with a full general circulation model. *Journal of Geophysical Research (Planets)*, 115:6006–+, June 2010b. doi: 10.1029/2009JE003458. v, 1, 2, 32, 59, 60

C. Lee. *Modelling of the Atmosphere of Venus*. PhD thesis, PhD Thesis, Oxford University, 2006. v, vii, 1, 7, 8, 9, 10, 11, 13, 17, 20, 60

C. Lee and M. I. Richardson. A discrete ordinate, multiple scattering, radiative transfer model of the Venus atmosphere from 0.1 to 50 microns. *In preparation*, 2010. 33

C. Lee, S. R. Lewis, and P. L. Read. Superrotation in a Venus general circulation model. *Journal of Geophysical Research (Planets)*, 112(E11):4–+, April 2007. doi: 10.1029/2006JE002874. 1, 7, 11, 20, 31

C. Lee, S. R. Lewis, and P. L. Read. A bulk cloud parameterization in a Venus General Circulation Model. *icarus*, 206:662–668, April 2010a. doi: 10.1016/j.icarus.2009.09.017. 10, 32

C. Lee, S. R. Lewis, and P. L. Read. A bulk cloud parameterization in a Venus General Circulation Model. *Icarus*, 206:662–668, April 2010b. doi: 10.1016/j.icarus.2009.09.017. 5

C. B. Leovy. Rotation of the upper atmosphere of Venus. *Journal of Atmospheric Sciences*, 30:1218–1220, 1973. doi: 10.1175/1520-0469(1973)030. 3

S. S. Limaye. Venus atmospheric circulation - Observations and implications of the thermal structure. *Advances in Space Research*, 5:51–62, 1985. doi: 10.1016/0273-1177(85)90270-4. 27, 28, 29, 57

S. S. Limaye, J. P. Kossin, C. Rozoff, G. Piccioni, D. V. Titov, and W. J. Markiewicz. Vortex circulation on Venus: Dynamical similarities with terrestrial hurricanes. *Geophys. Res. Lett.*, 36:4204–+, February 2009. doi: 10.1029/2008GL036093. 3

K. N. Liou. 1992. 37, 42, 43

K. N. Liou. 2002. 35, 50

S. Manabe and R. F. Strickler. Thermal Equilibrium of the Atmosphere with a Convective Adjustment. *Journal of Atmospheric Sciences*, 21:361–385, July 1964. doi: 10.1175/1520-0469(1964)021<0361:TEOTAW>2.0.CO;2. 46

K. B. McGouldrick. *Microphysics and Radiative-Dynamical Feedback in the Near Infrared Brightness Features in the Venus Clouds*. PhD thesis, PhD Thesis, University of Colorado, 2007. 42

C. P. McKay, J. B. Pollack, and R. Courtin. The thermal structure of Titan's atmosphere. *Icarus*, 80:23–53, July 1989. doi: 10.1016/0019-1035(89)90160-7. 12

V. I. Moroz, A. P. Ekonomov, B. E. Moshkin, H. E. Revercomb, L. A. Sromovsky, and J. T. Schofield. Solar and thermal radiation in the Venus atmosphere. *Advances in Space Research*, 5:197–232, 1985. doi: 10.1016/0273-1177(85)90202-9. 32

N. I. Moskalenko, I. A. Ilin, S. N. Parzhin, and L. V. Rodionov. Pressure-induced infrared radiation absorption in atmospheres. *Akademiia Nauk SSSR Fizika Atmosfery i Okeana*, 15:912–919, September 1979. 40, 42

T. Nakajima, M. Tsukamoto, Y. Tsushima, A. Numaguti, and T. Kimura. Modeling of the Radiative Process in an Atmospheric General Circulation Model. *Applied Optics*, 39:4869–4878, September 2000. doi: 10.1364/AO.39.004869. 59

M. Newman and C. Leovy. Maintenance of strong rotational winds in Venus' middle atmosphere by thermal tides. *Science*, 257:647–650, July 1992. doi: 10.1126/science.257.5070.647. 32

M. Newman, G. Schubert, A. J. Kliore, and I. R. Patel. Zonal winds in the middle atmosphere of Venus from Pioneer Venus radio occultation data. *Journal of Atmospheric Sciences*, 41:1901–1913, June 1984. doi: 10.1175/1520-0469(1984)041. 19, 23

A. Piccialli, D. V. Titov, D. Grassi, I. Khatuntsev, P. Drossart, G. Piccioni, and A. Migliorini. Cyclostrophic winds from the Visible and Infrared Thermal Imaging Spectrometer temperature sounding: A preliminary analysis. *Journal of Geophysical Research (Planets)*, 113(E12):0–+, October 2008. doi: 10.1029/2008JE003127. 19, 20, 23, 27

G. Piccioni, P. Drossart, A. Sanchez-Lavega, R. Hueso, F. W. Taylor, C. F. Wilson, D. Grassi, L. Zasova, M. Moriconi, A. Adriani, S. Lebonnois, A. Coradini, B. Bézard, F. Angrilli, G. Arnold, K. H. Baines, G. Bellucci, J. Benkhoff, J. P. Bibring, A. Blanco, M. I. Blecka, R. W. Carlson, A. di Lellis, T. Encrenaz, S. Erard, S. Fonti, V. Formisano, T. Fouchet, R. Garcia, R. Haus, J. Helbert, N. I. Ignatiev, P. G. J. Irwin, Y. Langevin, M. A. Lopez-Valverde, D. Luz, L. Marinangeli, V. Orofino, A. V. Rodin, M. C. Roos-Serote, B. Saggin, D. M. Stam, D. Titov, G. Visconti, M. Zambelli, E. Ammannito, A. Barbis, R. Berlin, C. Bettanini, A. Boccaccini, G. Bonnello, M. Bouye, F. Capaccioni, A. Cardesin Moinelo, F. Carraro, G. Cherubini, M. Cosi, M. Dami, M. de Nino, D. Del Vento, M. di Giampietro, A. Donati, O. Dupuis, S. Espinasse, A. Fabbri, A. Fave, I. F. Veltroni, G. Filacchione, K. Garceran, Y. Ghomchi, M. Giustini, B. Gondet, Y. Hello, F. Henry, S. Hofer, G. Huntzinger, J. Kachlicki, R. Knoll, K. Driss, A. Mazzoni, R. Melchiorri, G. Mondello, F. Monti, C. Neumann, F. Nuccilli, J. Parisot, C. Pasqui, S. Perferi, G. Peter, A. Piacentino, C. Pompei, J.-M. Reess, J.-P. Rivet, A. Romano, N. Russ, M. Santoni, A. Scarpelli, A. Semery, A. Soufflot, D. Stefanovitch, E. Suetta, F. Tarchi, N. Tonetti, F. Tosi, and B. Ulmer. South-polar features on Venus similar to those near the north pole. *Nature*, 450:637–640, November 2007. doi: 10.1038/nature06209. 3, 19

V. Ramanathan, R. J. Cicerone, J. T. Kiehl, and H. B. Singh. Trace gas trends and their potential role in climate change. *J. Geophys. Res.*, 90:5547–5566, June 1985. doi: 10.1029/JD090iD03p05547. 45

P. Rannou, S. Lebonnois, F. Hourdin, and D. Luz. Titan atmosphere database. *Advances in Space Research*, 36:2194–2198, 2005. doi: 10.1016/j.asr.2005.09.041. 12

P. L. Read. Super-rotation and diffusion of axial angular momentum. II. A review of quasi-axisymmetric models of planetary atmospheres. *Quarterly Journal of the Royal Meteorological Society*, 112:253–272, 1986. doi: 10.1256/smsqj.47113. 3

R. E. Roberts, L. M. Biberman, and J. E. A. Selby. Infrared continuum absorption by atmospheric water vapor in the 8-12-micron window. *Applied Optics*, 15:2085–2090, September 1976. 42, 43

W. B. Rossow and G. P. Williams. Large-scale motion in the Venus stratosphere. *Journal of Atmospheric Sciences*, 36:377–389, March 1979. doi: 10.1175/1520-0469(1979)036. 3

L. S. Rothman, R. B. Wattson, R. Gamache, J. W. Schroeder, and A. McCann. HITRAN HAWKS and HITEMP: high-temperature molecular database. In J. C. Dainty, editor, *Society of Photo-Optical Instrumentation Engineers (SPIE) Conference Series*, volume 2471 of *Presented at the Society of Photo-Optical Instrumentation Engineers (SPIE) Conference*, pages 105–111, June 1995. 32

L. S. Rothman, D. Jacquemart, A. Barbe, D. Chris Benner, M. Birk, L. R. Brown, M. R. Carleer, C. Chackerian, K. Chance, L. H. Coudert, V. Dana, V. M. Devi, J.-M. Flaud, R. R. Gamache, A. Goldman, J.-M. Hartmann, K. W. Jucks, A. G. Maki, J.-Y. Mandin, S. T. Massie, J. Orphal, A. Perrin, C. P. Rinsland, M. A. H. Smith, J. Tennyson, R. N. Tolchenov, R. A. Toth, J. Vander Auwera, P. Varanasi, and G. Wagner. The HITRAN 2004 molecular spectroscopic database. *Journal of Quantitative Spectroscopy and Radiative Transfer*, 96:139–204, December 2005. doi: 10.1016/j.jqsrt.2004.10.008. 32

G. Schubert. *General circulation and the dynamical state of the Venus atmosphere*, pages 681–765. 1983. 2, 3, 22, 61

A. Seiff. *Thermal structure of the atmosphere of Venus*, pages 215–279. 1983. 10

A. Seiff, D. B. Kirk, R. E. Young, R. C. Blanchard, J. T. Findlay, G. M. Kelly, and S. C. Sommer. Measurements of thermal structure and thermal contrasts in the atmosphere of Venus and related dynamical observations - Results from the four Pioneer Venus probes. *J. Geophys. Res.*, 85:7903–7933, December 1980. doi: 10.1029/JA085iA13p07903. 7, 10

F. W. Taylor, D. J. McCleese, and D. J. Diner. Polar clearing in the Venus clouds observed from the Pioneer Orbiter. *Nature*, 279:613–+, June 1979. doi: 10.1038/279613a0. 3, 22

N. A. Teanby, R. de Kok, P. G. J. Irwin, S. Osprey, S. Vinatier, P. J. Gierasch, P. L. Read, F. M. Flasar, B. J. Conrath, R. K. Achterberg, B. Bézard, C. A. Nixon, and S. B. Calcutt. Titan's winter polar vortex structure revealed by chemical tracers. *Journal of Geophysical Research (Planets)*, 113(12):12003–+, December 2008. doi: 10.1029/2008JE003218. 61

D. V. Titov, F. W. Taylor, H. Svedhem, N. I. Ignatiev, W. J. Markiewicz, G. Piccioni, and P. Drossart. Atmospheric structure and dynamics as the cause of ultraviolet markings in the clouds of Venus. *Nature*, 456:620–623, December 2008. doi: 10.1038/nature07466. v, 49, 61

M. G. Tomasko, L. R. Doose, P. H. Smith, and A. P. Odell. Measurements of the flux of sunlight in the atmosphere of Venus. *J. Geophys. Res.*, 85:8167–8186, December 1980. doi: 10.1029/JA085iA13p08167. 32, 38

M. G. Tomasko, L. R. Doose, and P. H. Smith. The absorption of solar energy and the heating rate in the atmosphere of Venus. *Advances in Space Research*, 5:71–79, 1985. doi: 10.1016/0273-1177(85)90272-8. 7

D. A. Warrilow, A. B. Sangster, and A. Slingo. Modeling of land surface processes and their influence on European climate. *Tech. Rep. DCTN 38, UKMO, Meteorological Office, London Road, Bracknell, Bershire, United Kingdom*, 1986. 46

E. W. Washburn. International Critical Tables of Numerical Data: Physics, Chemistry and Technology. *New York, NY: McGraw-Hill*. vii, 35

D. R. Williams. Earth fact sheet: National space science data center. *http://nssdc.gsfc.nasa.gov/planetary/factsheet/earthfact.html*, 2003a. 13

D. R. Williams. Venus fact sheet: National space science data center. *http://nssdc.gsfc.nasa.gov/planetary/factsheet/venusfact.html*, 2003b. 7, 13

M. Yamamoto, M Takahashi, K. Ikeda, M. Takahashi, and Y. Matsuda. Development of Venus GCM toward the AKATSUKI mission. 2010 VEXAG International Workshop, 2010. 59

L. V. Zasova, N. Ignatiev, I. Khatuntsev, and V. Linkin. Structure of the Venus atmosphere. *PlanSS*, 55:1712–1728, October 2007. doi: 10.1016/j.pss.2007.01.011. 40, 61